

Transition Metal Dichalcogenides Multijunction Solar Cells Toward the Multicolor Limit

Seungwoo Lee*

*Department of Integrated Energy Engineering (College of Engineering) & KU-KIST
Graduate School of Converging Science and Technology, Korea University, Seoul 02841,
Republic of Korea*

E-mail: seungwoo@korea.ac.kr

Abstract

Transition metal dichalcogenides (TMDs) and other van der Waals semiconductors enable transfer-printed, lattice-mismatch-free stacking of many photovoltaic junctions, motivating a re-examination of multijunction detailed-balance limits under realistic material and optical constraints. Here we develop an unlimited-junction detailed-balance framework for split-spectrum, multi-terminal vdW multijunction solar cells and apply it to a conservative TMD bandgap window (1.0–2.1 eV). Dynamic-programming optimization shows that the accessible bandgap window imposes a large- N efficiency limit: under full concentration, unconstrained ladders approach 84.5% at $N = 50$, whereas the TMD window plateaus near 63.4%. This plateau is set by photons outside the gaps, so radiative quality and optics dominate beyond five junctions for realistic transfer-printed stacks. We identify an experimentally achievable $N = 5$ ladder $E_g \approx (2.10, 1.78, 1.50, 1.24, 1.00)$ eV and map each rung to candidate vdW/TMD absorbers. Using reciprocity and luminescence thermodynamics, we quantify penalties from finite external radiative efficiency, two-sided emission, and luminescent coupling, and we introduce the upward-emitted luminescence power as a computable entropy-loss

proxy. Incorporating excitonic absorptance and nanophotonic thickness bounds yields practical thickness and light-management targets for transfer-printed stacks. Finally, inserting an idealized nonreciprocal multijunction model into the reciprocity-optimized ladders provides conservative headroom estimates, consistent with negligible benefit for single junctions but measurable gains for multijunction TMD stacks.

Keywords

multijunction photovoltaics; transition metal dichalcogenides; detailed balance; external radiative efficiency; luminescent coupling

1 Introduction

The Shockley–Queisser (SQ) detailed-balance limit for a single-junction solar cell formalizes the thermodynamic tradeoffs between (i) transmission loss from sub-bandgap photons, (ii) thermalization loss from above-bandgap photons, and (iii) radiative emission that reduces the achievable open-circuit voltage V_{oc} .¹ Multijunction photovoltaics mitigates these losses by partitioning the solar spectrum across multiple bandgaps.^{2,3} In the radiative and ideal-optics limit, the efficiency of multijunction devices approaches the reciprocal multicolor limit as the number of junctions grows.

Despite decades of progress, pushing beyond triple-junction stacks remains challenging in conventional epitaxial material systems because lattice matching, thermal expansion mismatch, and defect formation create practical constraints. Van der Waals semiconductors—especially TMDs—offer a fundamentally different integration pathway: their layered nature enables mechanical exfoliation, deterministic transfer printing, and assembly of many junctions without lattice matching.⁴ This raises a natural theoretical question: If we could stack an arbitrary number of vdW junctions, and if we could select bandgaps broadly across the solar spectrum, how close could we approach multicolor or even Landsberg-like limits?

Answering this question requires more than bandgap optimization. As emphasized by luminescence thermodynamics, high-efficiency photovoltaics must exhibit strong internal radiative recombination and high external photon extraction.⁵ Reciprocity further implies that absorption and emission are inseparable: thickness- and nanophotonics-controlled absorptance shapes not only the short-circuit current J_{sc} but also the radiative dark current and therefore V_{oc} .^{6,7} In stacked junctions without intermediate mirrors, an upper junction can emit externally both upward (to the environment) and downward (into the stack), which (i) opens additional optical emission channels and thus introduces an entropy/voltage penalty, and (ii) enables luminescent coupling to lower junctions. These coupling processes can create additional thermalization or entropic losses in the lower junctions, particularly when bandgaps are closely spaced and when the upper junction is highly radiative. Recent detailed-balance analyses of nanophotonic intermediate mirrors in tandem photovoltaics highlight that the net gain can be strongly context dependent, highlighting the need for stack-specific photon-entropy accounting.⁸

Motivated by this perspective, we pursue a conservative and practical goal: maximize the reciprocal multijunction efficiency achievable with a realistic TMD bandgap window (1.0–2.1 eV), and quantify how luminescence extraction and thickness constraints shape the approach to the multicolor limit. Nonreciprocal optics is treated as an optional strategy: we benchmark its theoretical headroom by applying the idealized nonreciprocal multijunction model of Fan et al.⁹ to the same bandgap ladders optimized under reciprocity (a conservative “plug-in” comparison), and we explicitly contrast this multijunction headroom with the absence of benefit in single-junction photovoltaics.¹⁰

Beyond bandgap engineering, system-level photonics layers can further reshape the spectral and angular photon budget in practical photovoltaics. Examples include luminescent solar concentrators for spectral management,¹¹ neutral-colored transparent crystalline-silicon photovoltaics,¹² and transparent radiative-cooling exterior films for outdoor deployment.¹³ These developments reinforce the motivation for a unified thermodynamic treatment of

emission, coupling, and thickness constraints when designing transfer-printed multijunction stacks.

2 Overview of the device concept and photon-flow constraints

Figure 1 sketches the transfer-printed vdW multijunction architecture considered here: a stack of independently contacted subcells assembled by vdW stacking or transfer printing, with selective contacts/interlayers between subcells, a transparent top electrode, and a reflective back electrode. Throughout, we focus on multi-terminal extraction (each subcell operates at its own maximum power point), which isolates the fundamental spectral-partitioning thermodynamics from current-matching constraints.

Two points are central. First, in the detailed-balance limit each junction is a light-emitting diode under forward bias: at open circuit and near maximum power, the device emits a substantial photon flux. Strong external luminescence is therefore not a loss to be suppressed, but a signature of a high-quality device approaching the SQ limit.⁵ Second, in a stacked architecture, the direction and angular distribution of luminescence matter. If an upper junction emits downward into the stack, that emission is not necessarily “wasted”—it can be re-absorbed by lower junctions (luminescent coupling). However, it can still introduce (i) a voltage penalty for the emitter by opening emission channels, and (ii) a thermalization penalty in the absorber if the photon energy significantly exceeds the lower-junction bandgap. A quantitative framework must therefore track both photon flux and power flux of luminescence.

3 Theory and Methods

3.1 Spectral model, concentration, and incident power

We model the sun as a blackbody at temperature T_s and the cell as a blackbody at temperature T_c (unless otherwise stated $T_s = 5778\text{ K}$ and $T_c = 300\text{ K}$). The spectral photon flux per unit area per unit energy per steradian is

$$\Phi_{\text{bb}}(E, T) = \frac{2E^2}{h^3 c^2} \frac{1}{\exp(E/k_B T) - 1}, \quad (1)$$

where E is photon energy, h is Planck's constant, and c is the speed of light. The sun subtends solid angle $\Omega_s = \pi \sin^2 \theta_s$ where $\theta_s \simeq 0.266$ degree is the solar half-angle. Optical concentration is represented by scaling the incident flux by a factor C , so that the spectral photon flux incident on the device is

$$\Phi_{\odot}(E) = C \Omega_s \Phi_{\text{bb}}(E, T_s). \quad (2)$$

The incident radiative power density is

$$P_{\text{in}}(C) = \int_0^{\infty} E \Phi_{\odot}(E) dE. \quad (3)$$

In “full concentration” we use $C = C_{\text{max}} = 1/\sin^2 \theta_s$ (consistent with the SQ convention in which the sun's étendue is expanded to π steradians).^{1,3} All numerical integrations are performed on an energy grid spanning 0.01 eV to 10 eV, which captures $\approx 98\%$ of the blackbody solar power for $T_s = 5778\text{ K}$.

3.2 Single-junction detailed balance

For an ideal diode, the current–voltage relation is

$$J(V) = J_{\text{sc}} - J_0 \left[\exp \left(\frac{qV}{k_B T_c} \right) - 1 \right], \quad (4)$$

where J_{sc} is the short-circuit current density and J_0 is the dark-current prefactor. For an absorber with absorptance $A(E)$ (not necessarily unity), the photogenerated current density is

$$J_{\text{sc}} = q \int_0^{\infty} A(E) \Phi_{\odot}(E) dE. \quad (5)$$

Radiative recombination produces an emitted photon flux proportional to $A(E) \Phi_{\text{bb}}(E, T_c)$ by Kirchhoff's law and reciprocity.⁶ Thus the radiative dark current is

$$J_{0,\text{rad}} = q \int_0^{\infty} A(E) \Phi_{\text{bb}}(E, T_c) \Omega_{\text{emit}} dE, \quad (6)$$

where Ω_{emit} is the emission solid angle. For one-sided emission (perfect back reflector), $\Omega_{\text{emit}} = 2\pi$, whereas two-sided emission corresponds to $\Omega_{\text{emit}} = 4\pi$.

Nonradiative recombination and parasitic optical loss reduce the fraction of recombination events yielding externally emitted photons. A convenient device-quality metric is the external radiative efficiency ERE, which can be introduced via

$$J_0 = \frac{J_{0,\text{rad}}}{\text{ERE}}. \quad (7)$$

At fixed J_{sc} , Eq. (7) produces a voltage penalty

$$\Delta V_{\text{ERE}} = \frac{k_B T_c}{q} \ln(\text{ERE}), \quad (8)$$

identical in form to the $\ln Q_e^{\text{LED}}$ term that appears in the thermodynamic voltage decomposition of Rau and co-workers.^{7,14,15}

The maximum power point (MPP) can be obtained analytically using the Lambert- W function. Starting from Eq. (4), the condition $d(VJ)/dV = 0$ leads to $(1 + v) \exp(v) = 1 + J_{\text{sc}}/J_0$ where $v = qV/(k_B T_c)$. This gives

$$v_{\text{mpp}} = W(e[1 + J_{\text{sc}}/J_0]) - 1, \quad (9)$$

with $V_{\text{mpp}} = (k_B T_c/q) v_{\text{mpp}}$ and $P_{\text{mpp}} = V_{\text{mpp}} J(V_{\text{mpp}})$. A full derivation is provided in the Supporting Information.

3.3 Unlimited-junction split-spectrum multijunction model

We consider an N -junction multijunction device with bandgaps $E_{g,1} > E_{g,2} > \dots > E_{g,N}$. In the split-spectrum/multi-terminal limit, junction i interacts with photon energies in a window $E \in [E_{g,i}, E_{g,i-1})$ where $E_{g,0} \equiv E_{\text{max}}$ is a numerical high-energy cutoff. For step absorbers, $A_i(E) = 1$ in this window and $A_i(E) = 0$ outside it. The total maximum power density is

$$P_{\text{tot}}^* = \sum_{i=1}^N P_i^*(E_{g,i}; E_{g,i-1}), \quad (10)$$

where P_i^* is obtained from Eqs. (5)–(9) restricted to the window. We compute optimal bandgap ladders by maximizing Eq. (10) with dynamic programming (DP) on a discretized bandgap grid (see Supporting Information). We report two scenarios: (i) unconstrained E_g (theoretical convergence), and (ii) a conservative, experimentally motivated TMD window $E_g \in [1.0, 2.1]$ eV.

3.4 Reciprocity, emission channels, and luminescent coupling in reciprocal stacks

The reciprocity relation between photovoltaic quantum efficiency and electroluminescent emission connects absorption and emission spectra.⁶ A compact form for the emitted photon

flux spectrum under bias V is

$$\phi_{\text{em}}(E, V) = A(E) \Phi_{\text{bb}}(E, T_c) \Omega_{\text{emit}} \left[\exp \left(\frac{qV}{k_B T_c} \right) - 1 \right], \quad (11)$$

where $A(E)$ is the device absorptance (or external PV quantum efficiency under ideal collection). Equation (11) makes explicit that any thickness- or nanophotonics-induced change in $A(E)$ affects both J_{sc} and $J_{0,\text{rad}}$.

In a reciprocal multijunction stack lacking intermediate mirrors, each junction can emit both upward and downward (two hemispheres). Allowing both hemispheres doubles the radiative dark current prefactor and produces a radiative-voltage reduction $\Delta V = (k_B T_c / q) \ln 2$ at fixed generation. More importantly, downward emission from junction i can be absorbed by junction $i + 1$ if $E_{g,i} > E_{g,i+1}$, producing a luminescent-coupling current J_{LC} . We model this effect using a minimal coupled detailed-balance chain (see Supporting Information) in which

$$J_i(V_i) = J_{\odot,i} + J_{\text{rad},i-1}^{\downarrow}(V_{i-1}) - \frac{J_{0,i}^{\uparrow} + J_{0,i}^{\downarrow}}{\text{ERE}_i} \left[\exp \left(\frac{qV_i}{k_B T_c} \right) - 1 \right], \quad (12)$$

$$J_{\text{rad},i}^{\downarrow}(V_i) = J_{0,i}^{\downarrow} \left[\exp \left(\frac{qV_i}{k_B T_c} \right) - 1 \right], \quad (13)$$

with $J_{\text{rad},0}^{\downarrow} \equiv 0$. This model captures (i) the emission-channel entropy penalty (two-sided emission increases J_0), and (ii) the photon recycling/coupling that can boost the lower-junction current. We solve for the system maximum power point by coordinate-ascent optimization over the set of subcell voltages $\{V_i\}$.

3.5 Entropy loss as upward-emitted luminescence power and coupling thermalization

A recurring conceptual challenge is to interpret luminescence in multijunction stacks: luminescence is both a necessity for high V_{oc} and a potential loss channel if emitted into non-useful

modes. To make this quantitative, we compute the upward-emitted luminescence power

$$P_{\text{lum}}^{\uparrow} = \sum_i \int E \phi_{\text{em},i}^{\uparrow}(E, V_i) dE, \quad (14)$$

and report $P_{\text{lum}}^{\uparrow}/P_{\text{in}}$ as an entropy-loss proxy for emission-channel losses. In reciprocal stacks without intermediate mirrors, $P_{\text{lum}}^{\uparrow}$ is nonzero because the stack must emit externally. In the idealized nonreciprocal model, $P_{\text{lum}}^{\uparrow}$ can be suppressed in multijunction architectures, enabling additional headroom.⁹

Downward luminescence, in contrast, is not necessarily lost: it can be absorbed by the next junction and partially converted to electrical work. However, the portion of downward luminescent power that exceeds the electrical work extracted by the lower junction becomes heat (thermalization). We compute a coupling-thermalization proxy,

$$P_{\text{therm}}^{\text{LC}} = \sum_{i=1}^{N-1} (P_{\text{lum},i}^{\downarrow} - V_{i+1} J_{\text{LC},i}), \quad (15)$$

where $P_{\text{lum},i}^{\downarrow}$ is the downward luminescent power emitted by junction i and $J_{\text{LC},i}$ is the corresponding coupling current absorbed by junction $i + 1$. In the Results, we use these definitions to separate upward entropy loss from coupling-induced thermalization for a representative $N = 5$ ladder.

3.6 Finite absorptance, excitonic TMD absorption, and thickness constraints

While the SQ limit assumes unity absorptance above E_g , real vdW absorbers are ultrathin. For TMDs, absorption is dominated by strong excitonic resonances and large absorption coefficients in the visible; nevertheless, tens-of-nanometers thickness is typically required to approach unity absorptance over broad spectral windows without strong light trapping.^{4,16} We therefore supplement the step-absorber model with a thickness-dependent absorptance

model

$$A(E; t) = 1 - \exp[-\alpha(E)L_{\text{eff}}(E)], \quad L_{\text{eff}}(E) = F(E) t, \quad (16)$$

where $\alpha(E)$ is the absorption coefficient and $F(E)$ is an optional path-length enhancement factor. To capture TMD-like spectral shape, we adopt a minimal excitonic absorption coefficient model consisting of an Urbach tail, a continuum onset, and A/B exciton peaks (see Supporting Information). Because reciprocity requires the same $A(E; t)$ in Eq. (6), thickness directly affects both J_{sc} and V_{oc} .

In the ultrathin regime, geometric-optics light-trapping factors (e.g., $4n^2$) may be overly optimistic. At an elementary level, the path-length enhancement factor is simply $F(E) = L_{\text{eff}}(E)/t$, i.e., the ratio between the average optical distance traveled by photons inside the absorber and the physical thickness t : $F(E) = 1$ describes a single-pass planar film, while $F(E) > 1$ captures multi-pass propagation and light trapping (back reflectors, resonant cavities, scattering/angle randomization, etc.). In thick absorbers with randomized ray directions, the broadband average is bounded by the Yablonovitch limit $F \leq 4n^2$, where n is the refractive index.¹⁷

When the thickness becomes comparable to the wavelength, however, light is better viewed as coupling through a finite set of radiative and guided modes, and the number of usable optical channels grows with thickness. Yu, Raman, and Fan derived wave-optics bounds on the maximum achievable enhancement in nanophotonic textures as a function of thickness and in-plane periodicity,¹⁷ and Miller emphasized the more general thickness-functionality connection for broadband optics.¹⁸ To capture this thickness-limited behavior without committing to a specific nanophotonic design, we introduce a normalized broadband enhancement function $g(t) \in [0, 1]$ and define a thickness-dependent path-length enhancement factor

$$F_{\text{proxy}}(t) = 1 + (4n^2 - 1) g(t), \quad (17)$$

so that $F_{\text{proxy}} = 1$ in the no-light-trapping limit and $F_{\text{proxy}} \rightarrow 4n^2$ only when sufficient

thickness (and optical degrees of freedom) is available. In this work we use $n = 4.5$ as a representative TMD value and take a simple saturating proxy $g(t) = 1 - \exp(-t/t_0)$ with $t_0 = 200$ nm (see Supporting Information). When using this proxy in Eq. (16) we approximate $F(E) \approx F_{\text{proxy}}(t)$, and we also discuss how wavelength-resolved bounds can be incorporated when a specific architecture is known (see Supporting Information).

4 Results

Efficiency versus junction number and the role of the bandgap window. Figure 2 summarizes the detailed-balance efficiency versus junction number N for (i) unconstrained bandgaps and (ii) the conservative TMD bandgap window (1.0–2.1 eV), under both 1 sun and full concentration. Under full concentration, the unconstrained efficiency increases from $\sim 40\%$ (single junction) to $\sim 70.7\%$ for $N = 5$ and $\sim 84.5\%$ by $N = 50$ (approaching the reciprocal multicolor limit). Imposing the TMD window yields a pronounced large- N plateau: $\sim 61.5\%$ for $N = 5$ and $\sim 63.4\%$ by $N = 50$. This plateau reflects an intrinsic materials constraint: once the accessible bandgap set no longer spans the entire solar spectrum, additional junctions provide diminishing returns.

Physically, the reciprocal multicolor limit is approached when the spectrum assigned to each junction becomes narrower as N increases, suppressing thermalization while maintaining a high radiative voltage under concentration. In the conservative TMD window, photons below 1.0 eV (near-IR) and above 2.1 eV (blue/UV) are irrevocably lost to transmission, so increasing N primarily repartitions the same limited spectral band. The rapid saturation by N on the order of five therefore implies that, within TMD-only bandgaps, further progress hinges more on luminescence quality (ERE), emission-channel control, and ultrathin optics than on pushing junction count. For example, under full concentration the TMD-window ladder rises from $\eta \approx 54.2\%$ at $N = 2$ to $\eta \approx 61.5\%$ at $N = 5$, whereas increasing junction count to $N = 10$ yields only $\eta \approx 63.4\%$ (Table 1).

Efficiency limit versus accessible bandgap window. To quantify how strongly the accessible bandgap window constrains large- N performance, Figure 3 maps the efficiency limit (here shown for $N = 20$ at full concentration) versus $(E_{g,\min}, E_{g,\max})$. The conservative TMD point (1.0–2.1 eV) lies far from an unconstrained optimum, explaining the plateau in Figure 2. This map provides a compact way to evaluate how expanding the accessible bandgap range (e.g., by including other vdW semiconductors beyond conventional TMDs, or by alloying/strain) could raise the plateau.

The map also highlights an asymmetry between extending the low-gap and high-gap edges. Lowering $E_{g,\min}$ generally yields a larger gain because the solar photon flux is high in the near-IR, whereas raising $E_{g,\max}$ mainly improves voltage and reduces high-energy thermalization for a smaller portion of the spectrum. This suggests that identifying a stable narrow-gap bottom absorber in the 0.8–1.0 eV range can provide disproportionate leverage, even if the top gap remains near 2 eV. Physically, the lower cutoff $E_{g,\min}$ directly sets the fraction of near-infrared photons that are transmitted without conversion; within a fixed-width window, extending $E_{g,\min}$ downward therefore provides a larger efficiency headroom than modestly increasing $E_{g,\max}$.

Optimal bandgap ladders and a representative $N = 5$ TMD design. Figure 4 shows optimal bandgap ladders for selected N within the conservative TMD window. As N increases, the ladder becomes denser, with the top junction pushed toward the maximum available gap (~ 2.1 eV) and the bottom junction pushed toward ~ 1 eV.

We adopt $N = 5$ as a representative experimentally achievable design (transfer-printed stacks beyond triple junction are a key motivation of this work). For $N = 5$ in the TMD window, the DP optimizer yields the ladder

$$E_g^{(N=5)} \approx (2.10, 1.78, 1.50, 1.24, 1.00) \text{ eV} \quad (\text{top} \rightarrow \text{bottom}). \quad (18)$$

This ladder is used throughout subsequent analyses of luminescence, coupling, and thickness.

Layer-resolved operating metrics for this representative $N = 5$ stack (including ERE and finite-absorptance effects) are provided in the Supporting Information (Figures S1 and S2).

For the representative $N=5$ ladder, the rung spacing is not uniform. The optimizer concentrates rungs where the solar spectrum has high photon flux, while keeping a comparatively wide spacing between the lowest two bandgaps. This nonuniformity matters beyond spectral splitting: in reciprocal stacks without intermediate mirrors, smaller bandgap spacing increases downward luminescent coupling and the associated thermalization burden in the lower cell. Thus, optical design choices that control two-sided emission can be as important as the bandgap selection itself.

Material mapping: candidate vdW/TMD absorbers for the $N = 5$ ladder. To connect target bandgaps to realizable absorbers, Figure 5 overlays representative optical gaps reported for a selection of vdW semiconductors and TMD thickness variants.^{4,16} The mapping is necessarily approximate because optical gaps depend on thickness, strain, dielectric environment, and exciton binding energy. Nevertheless, this comparison provides a practical starting point for selecting subcell candidates for transfer-printed stacks.

Two practical subtleties deserve emphasis when translating target optical gaps into device layers. First, monolayer TMD optical gaps are excitonic and depend on dielectric environment and strain, so the same nominal absorber can shift in both absorptance and radiative efficiency depending on encapsulation and adjacent layers. Second, many multilayer TMDs become indirect-gap as thickness increases, which can reduce luminescence and therefore reduce voltage unless light management and passivation mitigate nonradiative recombination.

Table 1 provides a compact rung-to-material mapping for the representative $N = 5$ ladder, emphasizing TMD-first choices within the conservative 1.0–2.1 eV window. The broader candidate database, including thickness/strain/alloy tunability ranges and optical-constant notes used in the thickness-dependent calculations, is provided in the Supporting Information (Tables S3–S6).

Among the five rungs, the bottom cell target near 1.0 eV is the most challenging within

Table 1: **Representative rung-to-material mapping for the $N = 5$ target ladder within the conservative 1.0–2.1 eV window.** Primary choices emphasize widely studied group-VI TMDs compatible with transfer printing; alternates illustrate thickness/strain/alloy routes and broader vdW options. See the Supporting Information, Tables S3–S6 for a more comprehensive candidate library and parameter notes.

Target E_g (eV)	Rung	Primary candidate	Alternates	Practical notes (tunability / caveats)
2.10	Top	WS ₂ (1L)	MoS ₂ (1L, strain/dielectric); HfS ₂ (few-L)	Wide-gap top cell; strong visible excitons; encapsulation and work-function control mitigate contact loss.
1.78	2	MoS ₂ (1L)	WS ₂ (2L–few-L); MoS _{2(1-x)} Se _{2x} (alloy)	Gap tunable by thickness and dielectric screening; prioritize high ERE and low series resistance.
1.50	3	MoSe ₂ (1L)	ReS ₂ ; WSe ₂ (1L, strain)	Mid-gap cell with strong excitonic absorption; minimize parasitic absorption in interlayers.
1.24	4	WSe ₂ (few-L/bulk)	MoS ₂ (bulk); InSe (few-L)	Near-IR edge; multilayer TMDs may become indirect; thickness increase can compensate finite absorptance.
1.00	Bottom	MoTe ₂ (few-L/bulk)	MoSe ₂ (bulk, ~1.1); BP (encapsulated, thickness-tuned)	Narrow-gap bottom cell; stability/oxidation and contact barriers require encapsulation and barrier-free contacts.

conventional TMDs and is also the most consequential for the efficiency limit because it controls near-IR photon capture. This makes contact engineering, encapsulation, and selection of narrow-gap vdW absorbers central to realizing the theoretical headroom.^{4,16,19}

System-level penalty from finite ERE. Figure 6 shows how efficiency degrades as ERE decreases below unity, for selected N values in the conservative TMD window. Because the voltage penalty is logarithmic, efficiencies remain relatively robust for ERE $\gtrsim 10^{-2}$ but decline rapidly for lower ERE. Importantly, in multijunction systems the penalty compounds across junctions: one low-ERE subcell can dominate the system loss.^{5,14,15} This motivates aggressive light-management and contact designs (low parasitic absorption, high-reflectivity mirrors, and low-loss transparent electrodes) that preserve external photon extraction in every subcell.

A simple quantitative rule-of-thumb illustrates the compounding nature of the loss: at room temperature, an ERE of 1e-2 corresponds to an open-circuit voltage penalty on the order of one tenth of a volt per junction, so a five-junction stack can lose several tenths of a volt in total even if current matching is ideal. This is why maintaining high ERE in every subcell (not only the top) is a prerequisite for approaching multicolor efficiencies. For the representative $N = 5$ ladder, reducing ERE from 1 to 10^{-2} lowers the full-concentration stack efficiency by about six absolute percentage points in the thick-limit regime (Figure 7).

Thickness dependence with excitonic TMD absorptance. Figure 7 moves beyond step absorbers to incorporate finite absorptance in ultrathin vdW layers. Panel (a) shows the excitonic absorption coefficient model used here, including A/B exciton peaks and a continuum onset; the model is intentionally minimal but captures the qualitative spectral features of many group-VI TMDs.^{4,16} The underlying optical-constant conventions (n , k , and α) and representative material parameters used in this work are summarized in the Supporting Information (Tables S2–S6). Panel (b) shows the resulting $N = 5$ stack efficiency versus a uniform subcell thickness t for ERE = 1 and ERE = 10^{-2} . Even though monolayer and few-layer TMDs exhibit pronounced excitonic absorption near the band edge, the usable solar spectrum spans a broad range of above-gap energies and the continuum absorption remains finite; consequently, a very thin film does not absorb all incident photons in a single pass. In the Beer–Lambert regime ($\alpha t \ll 1$), the absorptance scales approximately as $A \approx \alpha t$, so the short-circuit current and efficiency rise only gradually with thickness.

Using a 95% convergence criterion relative to the thick-absorber (step) limit for the full-concentration $N = 5$ ladder, the required thickness is ~ 120 nm per subcell for a single-pass geometry ($F = 1$). When broadband light trapping is included through the thickness-dependent proxy of Eq. (17)—i.e., $F(E) \approx F_{\text{proxy}}(t) > 1$ constructed from the normalized enhancement $g(t)$ in Figure 8c—this target thickness drops to ~ 20 nm. This shift provides an experimentally meaningful design message: moderate broadband path-length enhancement can trade *optical* thickness for *physical* thickness in ultrathin TMD stacks.

Finite absorptance imposes a double penalty in detailed balance. First, incomplete absorption directly reduces J_{sc} by allowing above-gap photons to transmit. Second, because the same absorptance weights radiative emission channels, reduced absorption increases the effective recombination-to-generation ratio that sets the voltage (the J_{sc}/J_0 ratio), lowering V_{mp} and the overall power. The proxy $F_{proxy}(t)$ accelerates convergence by increasing the effective photon dwell time, but it cannot make an arbitrarily thin absorber behave as a thick one: the normalized enhancement $g(t)$ is itself thickness-limited by nanophotonic channel counting and thickness-functionality bounds (Figure 8).^{17,18,20}

Nanophotonic bounds and the role of thickness. The need for a thickness-dependent broadband proxy follows from the distinction between geometric optics and wavelength-scale optics. In thick absorbers with randomized ray directions, the average internal path length can be increased up to the familiar Yablonovitch bound $F \leq 4n^2$. When $t \lesssim \lambda$, however, the optical response is mediated by a finite set of radiative and guided modes; the number of accessible channels (and therefore the achievable broadband response) grows with thickness. As a result, nanophotonic textures may yield strong enhancement at selected wavelengths or angles, but sustaining large enhancement over the broad solar spectrum is fundamentally thickness-limited.

Figure 8 summarizes representative results from nanophotonic light-trapping theory and motivates the normalized enhancement function $g(t)$ used throughout this work. Panel (a) illustrates the Yu–Raman–Fan wave-optics enhancement oscillations around the $4n^2$ limit for periodic textures, highlighting the discrete-channel nature of wavelength-scale light trapping.¹⁷ Panel (b) illustrates single-mode scaling trends emphasized in nanophotonic bounds.¹⁷ Panel (c) plots the simple saturating function $g(t)$ adopted here, which can be interpreted as the fraction of the $4n^2$ enhancement that is experimentally achievable as a broadband average at thickness t . We then construct the effective path-length enhancement factor $F_{proxy}(t) = 1 + (4n^2 - 1)g(t)$ [Eq. (17)], which is used in the absorptance model of Eq. (16) and in the thickness sweeps of Figure 7.^{18,20}

For multijunction stacks, this thickness constraint is wavelength selective: the longest-wavelength subcells are the hardest to enhance in the ultrathin regime, so the bottom junction often dictates the minimum practical thickness or the required strength of light trapping. Consequently, optical design should be co-optimized with the bandgap ladder, rather than treated as a post-processing step.¹⁸

Luminescent coupling and a power-budget view of entropy vs thermalization. Figure 9 quantifies when luminescent coupling becomes appreciable in reciprocal stacks and provides a power-budget decomposition for the representative $N = 5$ ladder. Panel (a) shows that the downward coupling current J_{LC} at the system MPP increases strongly with concentration and is amplified by high ERE via higher operating voltage. Panel (b) shows that the coupling ratio grows rapidly when adjacent bandgaps become closely spaced (small ΔE_g), a condition naturally approached in dense high- N ladders. Panel (c) provides a compact power budget for the representative $N = 5$ ladder: the upward luminescence power is plotted as an entropy-loss proxy, while coupling-induced thermalization is plotted separately. This decomposition clarifies the key design tension: suppressing upward emission can reduce entropy loss (and increase voltage), but downward emission into lower junctions can still create thermalization loss if energy is not efficiently converted.

Importantly, coupling is not universally detrimental. When the lower cell converts the coupled photons efficiently and the bandgap spacing is sufficiently large, downward luminescence can partially compensate current deficits and relax the need for perfect spectral splitting. However, in dense ladders with small bandgap spacing, coupled photons arrive with excess energy relative to the lower bandgap and are more likely to be dissipated as heat, effectively reintroducing a thermalization channel that grows with concentration and ERE. For the representative $N = 5$ ladder at full concentration, the reciprocal ideal-optics stack loses $\sim 1.24\%$ of the incident solar power as upward-emitted luminescence, whereas in the idealized nonreciprocal model this upward channel is eliminated and the electrical output increases by $\sim 1.5\%$ absolute, with part of the redirected luminescence appearing as

coupling-induced thermalization (Figure 9c).

Reciprocal vs nonreciprocal headroom (conservative “plug-in” comparison). Nonreciprocal multijunction photovoltaics has been proposed as a route to approach the Landsberg limit by suppressing entropy losses associated with reciprocal emission pathways.⁹ However, for single-junction solar cells, nonreciprocity does not increase the SQ efficiency limit under detailed balance.¹⁰ To place these insights in the present context, we benchmark the potential headroom by applying the idealized nonreciprocal multijunction model to the same bandgap ladders optimized under reciprocity (Option A, conservative comparison).

Figure 10 compares full-concentration efficiencies versus N for reciprocal and nonreciprocal cases, for both unconstrained bandgaps and the conservative TMD window. In the TMD window, the reciprocal efficiency plateaus near $\sim 63.4\%$ at large N , whereas the nonreciprocal model rises to $\sim 67.7\%$ at $N = 50$ (Figure 10a). Figure 10b shows the central physical signature: the nonreciprocal model suppresses upward-emitted luminescence power (entropy-loss proxy), whereas the reciprocal case must emit upward to maintain detailed balance. The filled markers in Figure 10a further show that reciprocal stacks without intermediate mirrors incur additional penalties from two-sided emission and coupling, highlighting the practical importance of intermediate mirrors or angular filters in realistic reciprocal designs.

In the conservative Option A comparison, the nonreciprocal model is applied to the reciprocity-optimized ladder without re-optimizing bandgaps, so the improvement should be interpreted as a lower bound on the possible headroom. In practice, achieving the ideal nonreciprocal behavior is nontrivial, but the comparison clarifies what must be suppressed in reciprocal stacks: upward emission that carries entropy, and downward emission that drives coupling thermalization. Intermediate mirrors, angular filters, and spectral-selective contacts can address part of this gap without requiring fully nonreciprocal photonics.

5 Discussion: design rules for transfer-printed vdW/TMD multijunction photovoltaics

We summarize design rules suggested by the above results.

- (1) **Bandgap-ladder engineering is necessary but not sufficient.** The DP optimizer provides optimal ladders and reveals the large- N plateau imposed by a constrained bandgap window. Within the conservative 1.0–2.1 eV TMD window, $N \approx 5$ already approaches the plateau, suggesting that the most immediate experimental objective is to realize high-quality $N \leq 5$ stacks with excellent optics rather than extremely large N .
- (2) **ERE is a system-level requirement.** Voltage penalties from finite ERE accumulate across subcells (Figure 6). High- N stacks therefore demand high radiative quality in every junction, reinforcing the importance of passivation, low-loss contacts, and photon extraction.^{5,15}
- (3) **Control of emission channels and luminescent coupling is essential.** Without intermediate mirrors, two-sided emission introduces an entropy penalty and enables downward luminescent coupling (Figure 9a–b). Coupling can be beneficial for current in lower cells but also introduces thermalization losses and can reduce the emitter voltage. Practical multijunction architectures will likely require selective optical elements (intermediate mirrors, angular filters, or photonic cavities) designed to maximize useful coupling while minimizing entropy penalties.^{7,8,17}
- (4) **Thickness and nanophotonics cannot be ignored in vdW stacks.** Ultrathin absorbers cannot be treated as step absorbers; finite absorptance reduces both J_{sc} and V_{oc} through reciprocity (Figure 7). Nanophotonic bounds and thickness constraints limit the achievable broadband path-length enhancement (Figure 8). These effects motivate moderate

absorber thicknesses (tens to hundreds of nm) and co-designed photonic structures rather than extreme monolayer limits for high-efficiency multijunction conversion.

(5) Nonreciprocity is an optional asymptotic strategy with multijunction-specific benefits. Consistent with Fan et al., nonreciprocity does not improve the SQ limit for single-junction devices.¹⁰ In multijunction architectures, however, reshaping emission pathways can reduce entropy losses and provide headroom toward Landsberg-like limits.⁹ Our conservative plug-in comparison (Figure 10) quantifies this headroom for TMD-optimized ladders while preserving the paper’s main focus: reciprocal multijunction design and realistic constraints.

6 Conclusions

We developed an unlimited-junction detailed-balance framework tailored to transfer-printed vdW/TMD multijunction photovoltaics and used it to compute optimal bandgap ladders under unconstrained and conservative TMD bandgap windows. A realistic bandgap window produces a large- N efficiency plateau, motivating $N \sim 5$ as a practical near-term target for TMD-based stacks. We incorporated luminescence thermodynamics and reciprocity to quantify ERE penalties, emission-channel entropy, and luminescent coupling, and we introduced a power-budget view in which upward-emitted luminescence serves as a directly computable entropy-loss proxy while coupling thermalization is tracked separately. Finally, we benchmarked the remaining thermodynamic headroom by applying an idealized nonreciprocal multijunction model to our reciprocally optimized ladders, showing negligible benefit for single junctions but substantial headroom for multijunction stacks. These results provide quantitative design rules for approaching multicolor efficiencies with transfer-printed vdW multijunction photovoltaics.

Data and code availability

The numerical results and figures in this work are reproducible from the Python implementation of the detailed-balance, luminescent-coupling, and optimization models described in the main text and Supporting Information. To keep the manuscript self-contained for submission, the Supporting Information includes the full derivations, parameter tables, and additional figures. The Python source code and the raw numerical data required to regenerate every figure and table are available from the authors upon reasonable request and will be deposited in a public repository upon publication.

Supporting Information

The Supporting Information (SI) is provided as a separate PDF file. The SI provides detailed derivations, parameter tables, and additional figures that support the main text: (i) Supporting Information, Section 1 (Constants, geometry, and spectral model): solar/blackbody spectral definitions and constants; (ii) Supporting Information, Section 2 (Single-junction detailed balance): full detailed-balance derivations, including the Lambert- W maximum-power condition; (iii) Supporting Information, Section 3 (Unlimited-junction split-spectrum multijunction model): the dynamic-programming (DP) optimizer used to compute optimal bandgap ladders for arbitrary N and its discretization/convergence checks; (iv) Supporting Information, Section 4 (Reciprocity, emission channels, and the role of mirrors): reciprocity-based voltage-loss and entropy-loss decompositions, including the role of external radiative efficiency (ERE) and optical outcoupling; (v) Supporting Information, Section 5 (Luminescent coupling chain model): the luminescent-coupling chain model, together with the definition and computation of the upward emitted luminescence power and a coupling thermalization/heat proxy; (vi) Supporting Information, Section 6 (TMD optical response and excitonic absorptance model): a TMD material database (representative bandgaps, excitonic absorption spectra, and representative $n(\lambda)/k(\lambda)$ dispersion conventions) and mapping of

candidate stacks to the representative $N = 5$ target ladder; (vii) Supporting Information, Section 7 (Nanophotonic bounds and Miller thickness constraints): nanophotonic bounds and thickness constraints relevant to ultrathin absorbers; (viii) Supporting Information, Section 8 (Nonreciprocal multijunction benchmark); (ix) Supporting Information, Section 9 (Extended bandgap-ladder tables for reproducibility); (x) Supporting Information, Section 10 (Additional figures for the representative $N = 5$ stack; Figures S1 and S2); (xi) Supporting Information, Section 11 (Full ladder lists in text form).

Author Information

Corresponding Author

Seungwoo Lee — E-mail: seungwoo@korea.ac.kr

Author Contributions

S.L. conceived the original research idea at the initial stage, computed all the results, and wrote the paper.

Notes

The author declares no competing financial interest.

Acknowledgments

We acknowledge funding from National Research Foundation of Korea (RS-2022-NR068141) and from the KIST Institutional Program (Project No.: 2V09840-23-P023). This research was also supported by a grant of the Korea-US Collaborative Research Fund (KUCRF),

funded by the Ministry of Science and ICT and Ministry of Health & Welfare, Republic of Korea (grant number: RS-2024-00468463) and by Korea University grant.

References

- (1) Shockley, W.; Queisser, H. J. Detailed Balance Limit of Efficiency of p-n Junction Solar Cells. *Journal of Applied Physics* **1961**, *32*, 510–519.
- (2) De Vos, A. Detailed balance limit of the efficiency of tandem solar cells. *Journal of Physics D: Applied Physics* **1980**, *13*, 839–846.
- (3) Green, M. A. Efficiency limits for single-junction and tandem solar cells. *Progress in Photovoltaics: Research and Applications* **2006**, *14*, 383–395.
- (4) Jariwala, D.; Davoyan, A. R.; Wong, J.; Atwater, H. A. Van der Waals Materials for Atomically-Thin Photovoltaics: Promise and Outlook. *ACS Photonics* **2017**, *11*, 53–61.
- (5) Miller, O. D.; Yablonovitch, E. Strong internal and external luminescence as solar cells approach the Shockley–Queisser limit. *IEEE Journal of Photovoltaics* **2012**, *2*, 303–311.
- (6) Rau, U. Reciprocity relation between photovoltaic quantum efficiency and electroluminescent emission of solar cells. *Physical Review B* **2007**, *76*, 085303.
- (7) Rau, U.; Paetzold, U. W.; Kirchartz, T. Thermodynamics of light management in photovoltaic devices. *Physical Review B* **2014**, *90*, 035211.
- (8) Kim, K.; Lee, J.; Lee, J.; Kim, J.-Y.; Lee, H.-S.; Lee, S. Are nanophotonic intermediate mirrors really effective in enhancing the efficiency of perovskite tandem solar cells? *Nanophotonics* **2025**, *14*, 1239–1248.
- (9) Park, Y.; Zhao, B.; Fan, S. Reaching the Ultimate Efficiency of Solar Energy Harvesting with a Nonreciprocal Multijunction Solar Cell. *Nano Letters* **2022**, *22*, 448–452.

(10) Park, Y.; Fan, S. Does Non-Reciprocity Break the Shockley–Queisser Limit in Single-Junction Solar Cells? *Applied Physics Letters* **2022**, *121*, 111102.

(11) Lee, S. H.; Baek, D.; Cho, W.; Lee, N.; Kim, K.; Kim, J.-H.; Kim, H.-J.; Kim, H. H.; Kim, H. J.; Lee, S.; Lee, S.-M. Tailoring Luminescent Solar Concentrators for High-Performance Flexible Double-Junction III-V Photovoltaics. *Advanced Functional Materials* **2023**, *33*, 2210357.

(12) Lee, K.; Kim, N.; Kim, K.; Um, H. D.; Jin, W.; Choi, D.; Park, J.; Park, K. J.; Lee, S.; Seo, K. Neutral-Colored Transparent Crystalline Silicon Photovoltaics. *Joule* **2020**, *4*, 235–246.

(13) Cho, Y.; Kim, H. H.; Ahn, S.; Lee, J.; Lee, J.; Kim, K.; Kwak, S.; Lee, H.; Choi, K.; Song, K.; Lee, S. Colloidal Opaline Composites as Throughput-Scalable, Fully Transparent, and Color-Tunable Radiative Cooling Exterior Films for Outdoor Photovoltaics. *Advanced Functional Materials* **2025**, *35*, e10833.

(14) Rau, U.; Kirchartz, T. Efficiency potential of photovoltaic materials and devices unveiled by detailed-balance analysis. *Physical Review B* **2017**, *95*, 245201.

(15) Kirchartz, T.; Rau, U. What makes a good solar cell? *Advanced Energy Materials* **2018**, *8*, 1703385.

(16) Reich, N.; Yu, Y.; Furchi, M.; others Efficiency limit of transition metal dichalcogenide solar cells. *Communications Physics* **2023**, *6*, 1–11.

(17) Yu, Z.; Raman, A.; Fan, S. Fundamental limit of nanophotonic light trapping in solar cells. *Proceedings of the National Academy of Sciences* **2010**, *107*, 17491–17496.

(18) Miller, D. A. B. Why optics needs thickness. *Science* **2023**, *380*, 742–746.

(19) Zhou, Z.; Lv, J.; Tan, C.; Yang, L.; Wang, Z. Emerging Frontiers of 2D Transition Metal

Dichalcogenides in Photovoltaics Solar Cell. *Advanced Functional Materials* **2024**, *34*, 2316175.

(20) Kim, K.; Lee, S. Detailed balance analysis of plasmonic metamaterial perovskite solar cells. *Optics Express* **2019**, *27*, A1241–A1260.

List of Figures

1	Conceptual schematic of a transfer-printed vdW/TMD multijunction solar cell (representative $N = 5$ ladder). In a reciprocal stack without intermediate mirrors, external luminescence from an upper junction can exit upward ($\Phi_{\text{ext}}^{\uparrow}$) and propagate downward ($\Phi_{\text{ext}}^{\downarrow}$), enabling luminescent coupling to lower junctions and opening additional emission channels (entropy/voltage penalty). Intermediate mirrors or angular filters can suppress unwanted emission channels and recover higher radiative voltage. ^{5,7} An optional nonreciprocal optical layer can, in principle, further reshape emission pathways and access additional thermodynamic headroom in multijunction stacks. ⁹	28
2	Detailed-balance efficiency versus junction number. (a) 1 sun and (b) full concentration for unconstrained optimal bandgaps and a conservative TMD bandgap window (1.0–2.1 eV), computed for split-spectrum (multi-terminal) multijunctions with one-sided emission and ERE = 1. Numerical tables and bandgap ladders are provided in the SI and the accompanying code package.	29
3	Efficiency limit versus accessible bandgap window. Heatmap of the maximum achievable efficiency for a representative high- N case ($N = 20$, multi-terminal, ERE = 1, full concentration), as a function of the allowed bandgap window ($E_{g,\text{min}}, E_{g,\text{max}}$). The conservative TMD window (1.0–2.1 eV) is highlighted.	30
4	Optimal bandgap ladders in the conservative TMD window. $E_{g,i}$ vs subcell index for selected N values (top cell is index 1). The $N = 5$ ladder in Eq. (18) is highlighted as a representative design.	31
5	Illustrative mapping between target bandgaps and vdW/TMD candidates. Symbols denote representative optical gaps drawn from the vdW/TMD literature (see Supporting Information, Table S3 for notes and sources), and dashed vertical lines denote the representative $N = 5$ target ladder (Eq. (18)).	32
6	Efficiency versus external radiative efficiency (ERE) in the TMD window. Efficiency computed for $N = 1, 2, 5$ under 1 sun (solid) and full concentration (dashed), illustrating the SQ-triangle voltage penalty and its correspondence to the thermodynamic Q_e^{LED} term. ^{7,14}	33
7	Thickness dependence for an $N = 5$ TMD multijunction stack with excitonic absorptance. (a) Example absorption coefficient model $\alpha(E)$ for a representative bandgap ($E_g = 1.78$ eV) including A/B exciton peaks and a continuum onset. (b) Total $N = 5$ stack efficiency under full concentration versus uniform subcell thickness t , comparing single-pass absorption ($F = 1$) to the thickness-dependent broadband light-trapping proxy $F_{\text{proxy}}(t)$ of Eq. (17). Reciprocity is enforced by using the same $A(E; t)$ in both J_{sc} and the radiative dark current.	34

8	Nanophotonic bounds and a broadband path-length enhancement proxy. (a) Channel-counting proxy illustrating deviations from the geometric-optics $4n^2$ limit in the wavelength-scale regime. (b) Single-mode scaling proxy for $F_{\max}/(4n^2)$ versus normalized thickness $\tau = d/(\lambda/2n)$. (c) Normalized broadband enhancement $g(t) = (F_{\text{proxy}}(t) - 1)/(4n^2 - 1)$ used to construct the thickness-dependent path-length enhancement factor $F_{\text{proxy}}(t) = 1 + (4n^2 - 1)g(t)$ in Figure 7. ^{17,18,20}	35
9	Luminescent coupling conditions and entropy/thermalization power budget. (a) Downward luminescent coupling current at MPP increases strongly with optical concentration and is larger for higher ERE. (b) Coupling ratio $\gamma = J_{\text{LC}}/J_{\odot,2}$ increases rapidly as the bandgap spacing decreases. (c) Power-budget decomposition for the representative $N = 5$ ladder under full concentration, comparing reciprocal ideal optics (no coupling), reciprocal stacks without intermediate mirrors (two-sided emission + coupling), and an idealized nonreciprocal model. Upward-emitted luminescence is shown as an entropy-loss proxy; coupling thermalization quantifies luminescent power not convertible to electrical work in the lower junctions.	36
10	Reciprocal vs nonreciprocal headroom under full concentration. (a) Efficiency versus junction number for reciprocal split-spectrum multijunctions (one-sided emission, no coupling), and for the idealized nonreciprocal multijunction model of Fan et al. ⁹ applied to the same reciprocity-optimized bandgap ladders (Option A). Filled markers show a reciprocal-stack estimate without intermediate mirrors (two-sided emission + downward luminescent coupling) for $N \leq 10$. (b) Upward-emitted luminescence power fraction $P_{\text{lum}}^{\uparrow}/P_{\text{in}}$ as an entropy-loss proxy. In the idealized nonreciprocal model used here, the upward-emitted luminescence is identically zero, so the nonreciprocal series in (b) are shown with a slight horizontal offset for visibility. Horizontal lines indicate literature multicolor and Landsberg limits for comparison (values depend weakly on T_s). ⁹	37

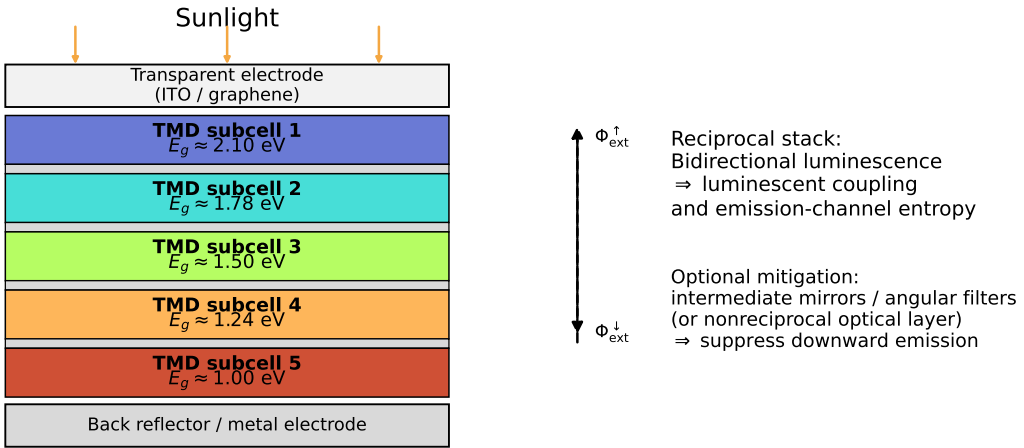


Figure 1: Conceptual schematic of a transfer-printed vdW/TMD multijunction solar cell (representative $N = 5$ ladder). In a reciprocal stack without intermediate mirrors, external luminescence from an upper junction can exit upward ($\Phi_{\text{ext}}^{\uparrow}$) and propagate downward ($\Phi_{\text{ext}}^{\downarrow}$), enabling luminescent coupling to lower junctions and opening additional emission channels (entropy/voltage penalty). Intermediate mirrors or angular filters can suppress unwanted emission channels and recover higher radiative voltage.^{5,7} An optional nonreciprocal optical layer can, in principle, further reshape emission pathways and access additional thermodynamic headroom in multijunction stacks.⁹

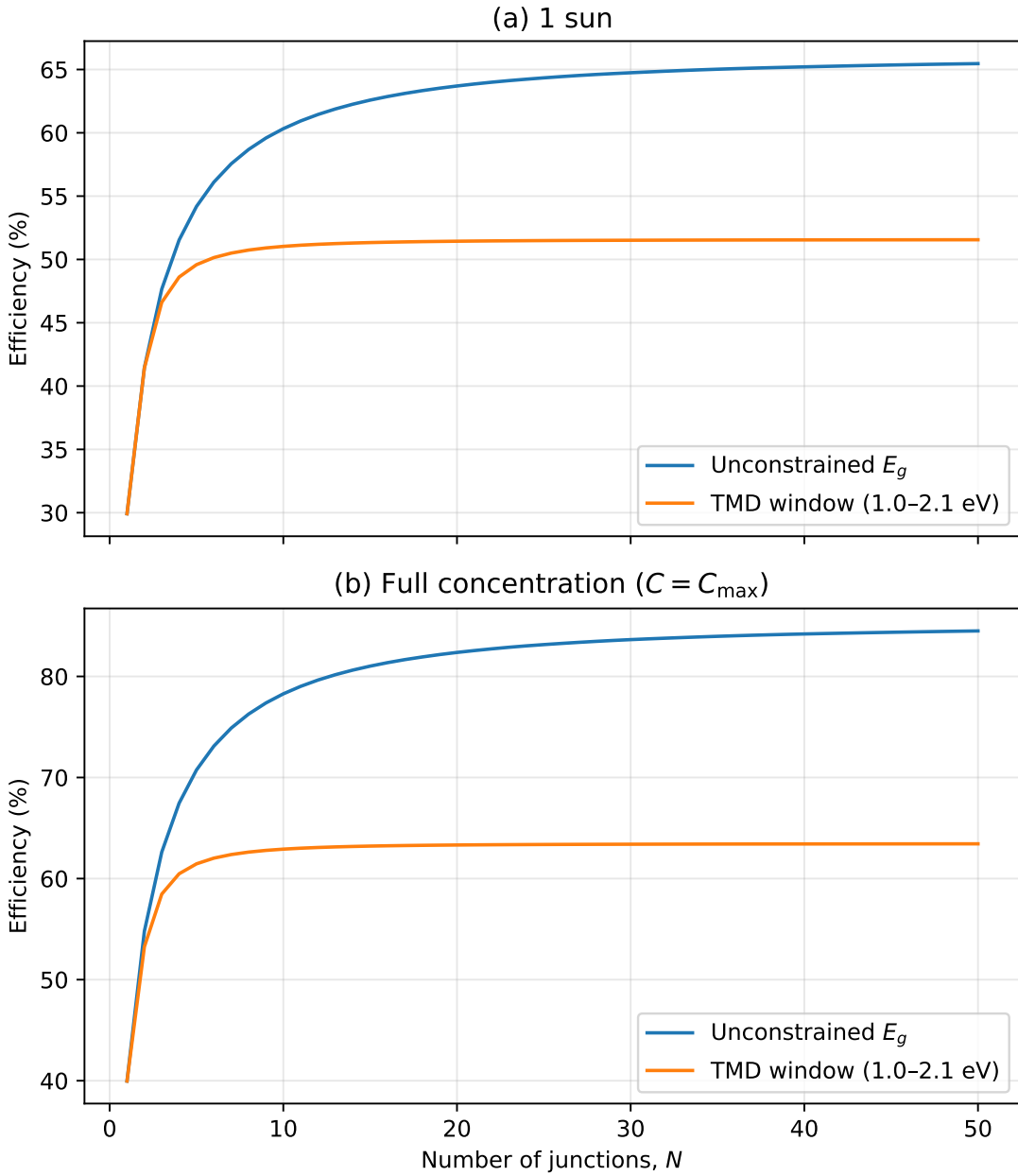


Figure 2: **Detailed-balance efficiency versus junction number.** (a) 1 sun and (b) full concentration for unconstrained optimal bandgaps and a conservative TMD bandgap window (1.0–2.1 eV), computed for split-spectrum (multi-terminal) multijunctions with one-sided emission and ERE = 1. Numerical tables and bandgap ladders are provided in the SI and the accompanying code package.

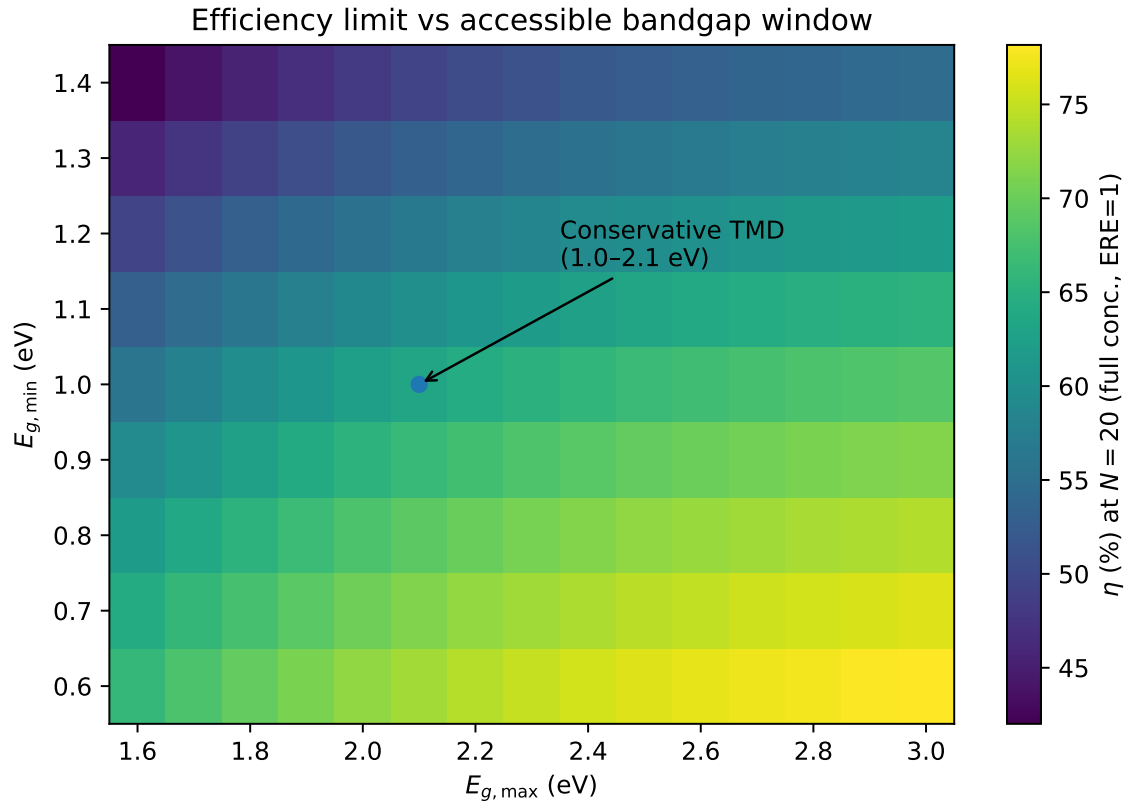


Figure 3: **Efficiency limit versus accessible bandgap window.** Heatmap of the maximum achievable efficiency for a representative high- N case ($N = 20$, multi-terminal, ERE = 1, full concentration), as a function of the allowed bandgap window ($E_{g,\min}, E_{g,\max}$). The conservative TMD window (1.0–2.1 eV) is highlighted.

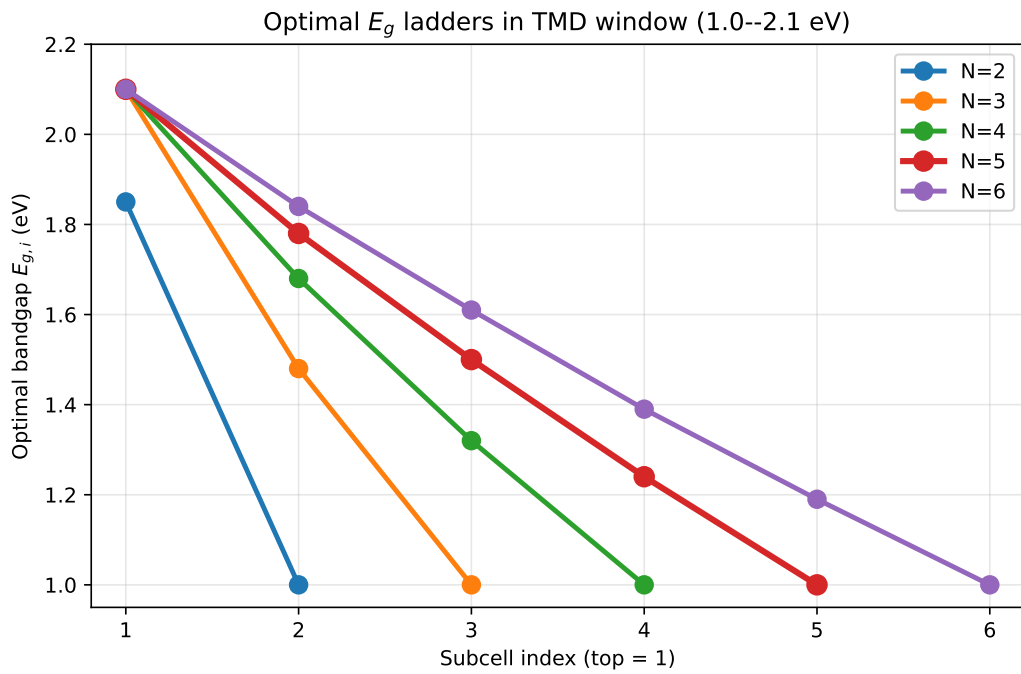


Figure 4: **Optimal bandgap ladders in the conservative TMD window.** $E_{g,i}$ vs subcell index for selected N values (top cell is index 1). The $N = 5$ ladder in Eq. (18) is highlighted as a representative design.

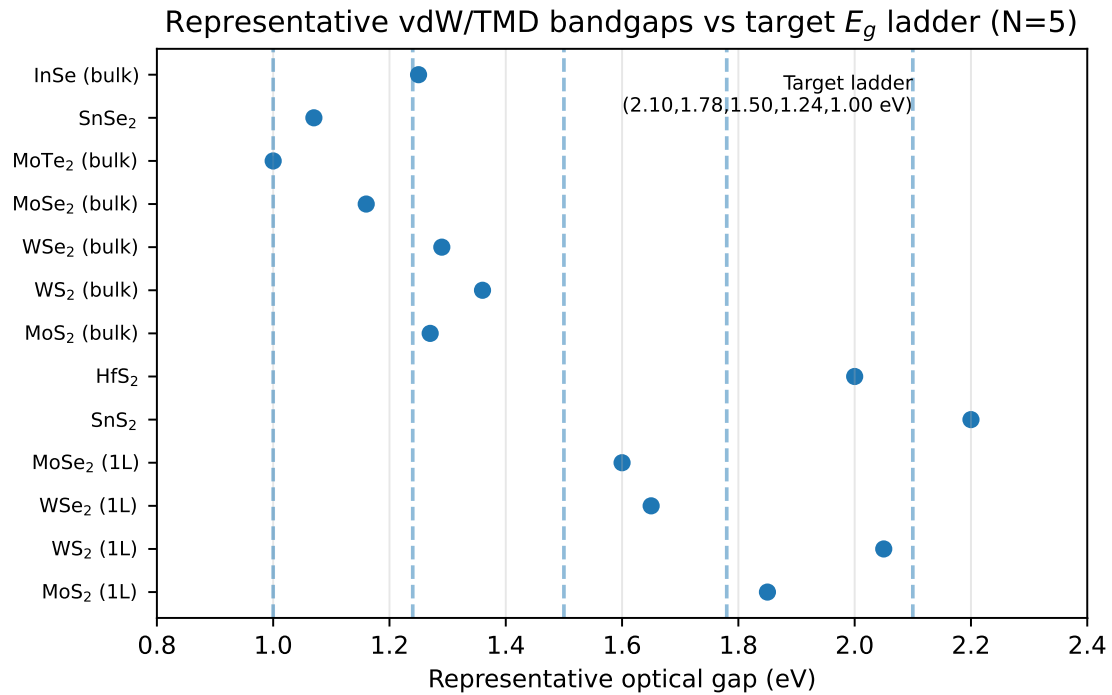


Figure 5: **Illustrative mapping between target bandgaps and vdW/TMD candidates.** Symbols denote representative optical gaps drawn from the vdW/TMD literature (see Supporting Information, Table S3 for notes and sources), and dashed vertical lines denote the representative $N = 5$ target ladder (Eq. (18)).

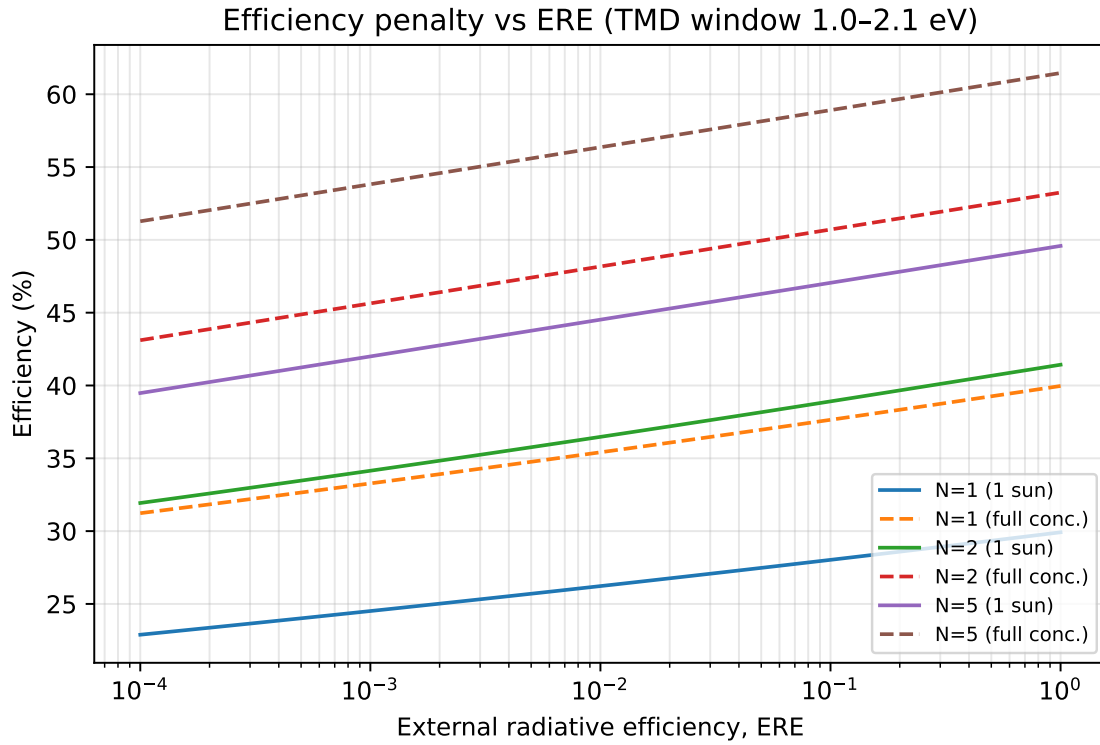


Figure 6: **Efficiency versus external radiative efficiency (ERE) in the TMD window.** Efficiency computed for $N = 1, 2, 5$ under 1 sun (solid) and full concentration (dashed), illustrating the SQ-triangle voltage penalty and its correspondence to the thermodynamic Q_e^{LED} term.^{7,14}

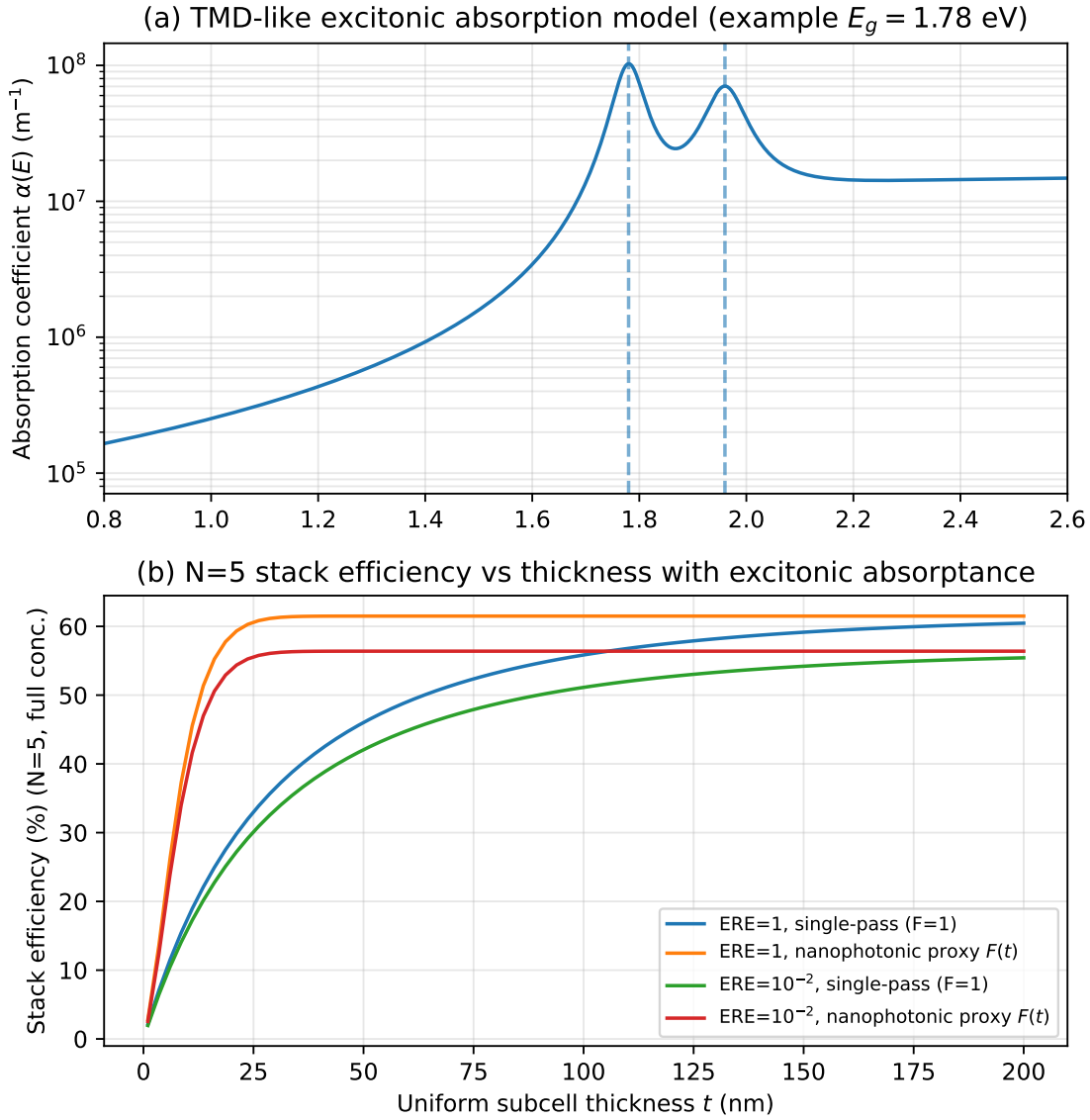


Figure 7: **Thickness dependence for an $N = 5$ TMD multijunction stack with excitonic absorptance.** (a) Example absorption coefficient model $\alpha(E)$ for a representative bandgap ($E_g = 1.78$ eV) including A/B exciton peaks and a continuum onset. (b) Total $N = 5$ stack efficiency under full concentration versus uniform subcell thickness t , comparing single-pass absorption ($F = 1$) to the thickness-dependent broadband light-trapping proxy $F_{\text{proxy}}(t)$ of Eq. (17). Reciprocity is enforced by using the same $A(E; t)$ in both J_{sc} and the radiative dark current.

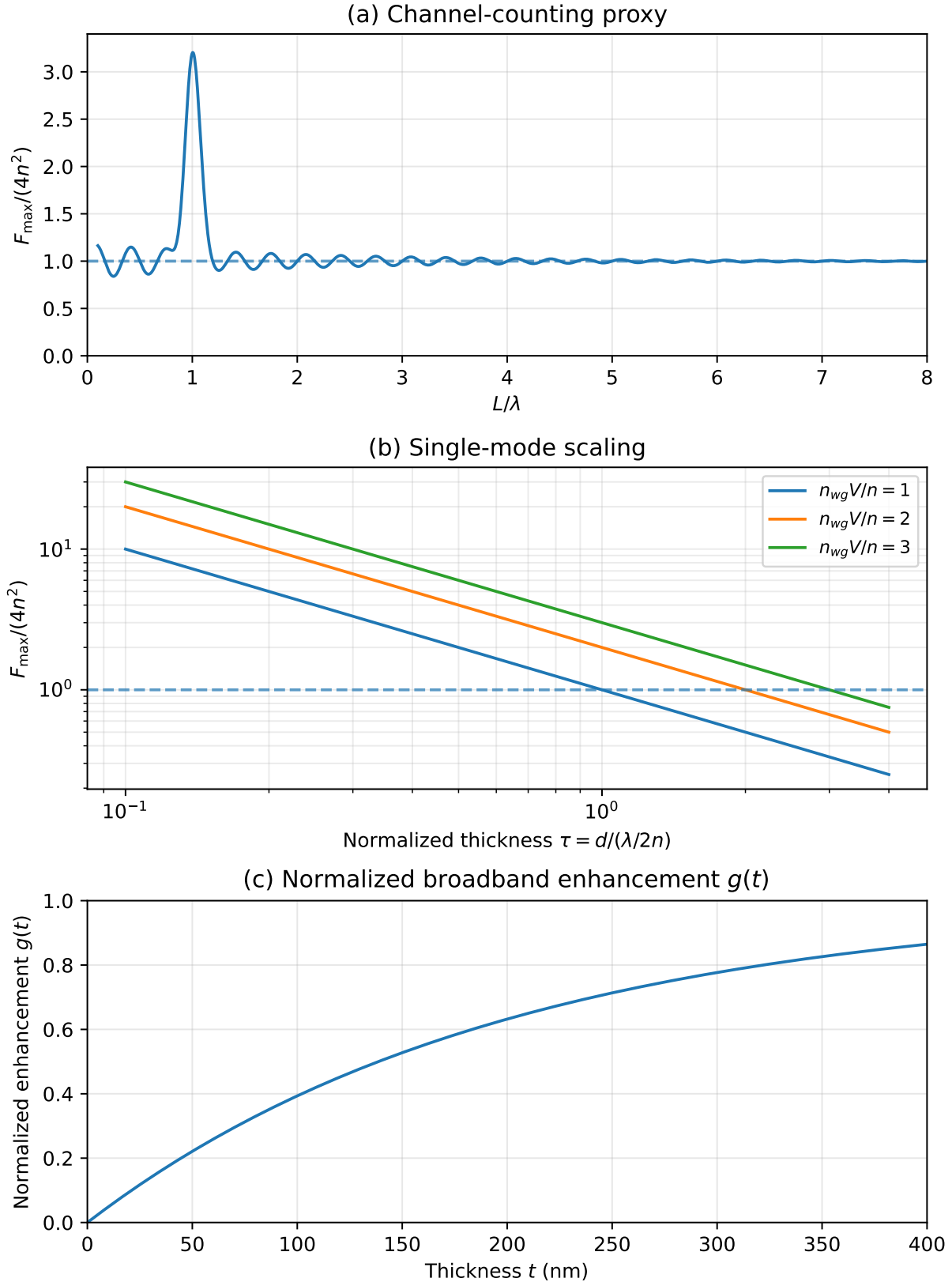


Figure 8: **Nanophotonic bounds and a broadband path-length enhancement proxy.** (a) Channel-counting proxy illustrating deviations from the geometric-optics $4n^2$ limit in the wavelength-scale regime. (b) Single-mode scaling proxy for $F_{\max}/(4n^2)$ versus normalized thickness $\tau = d/(\lambda/2n)$. (c) Normalized broadband enhancement $g(t) = (F_{\text{proxy}}(t) - 1)/(4n^2 - 1)$ used to construct the thickness-dependent path-length enhancement factor $F_{\text{proxy}}(t) = 1 + (4n^2 - 1)g(t)$ in Figure 7.^{17,18,20}

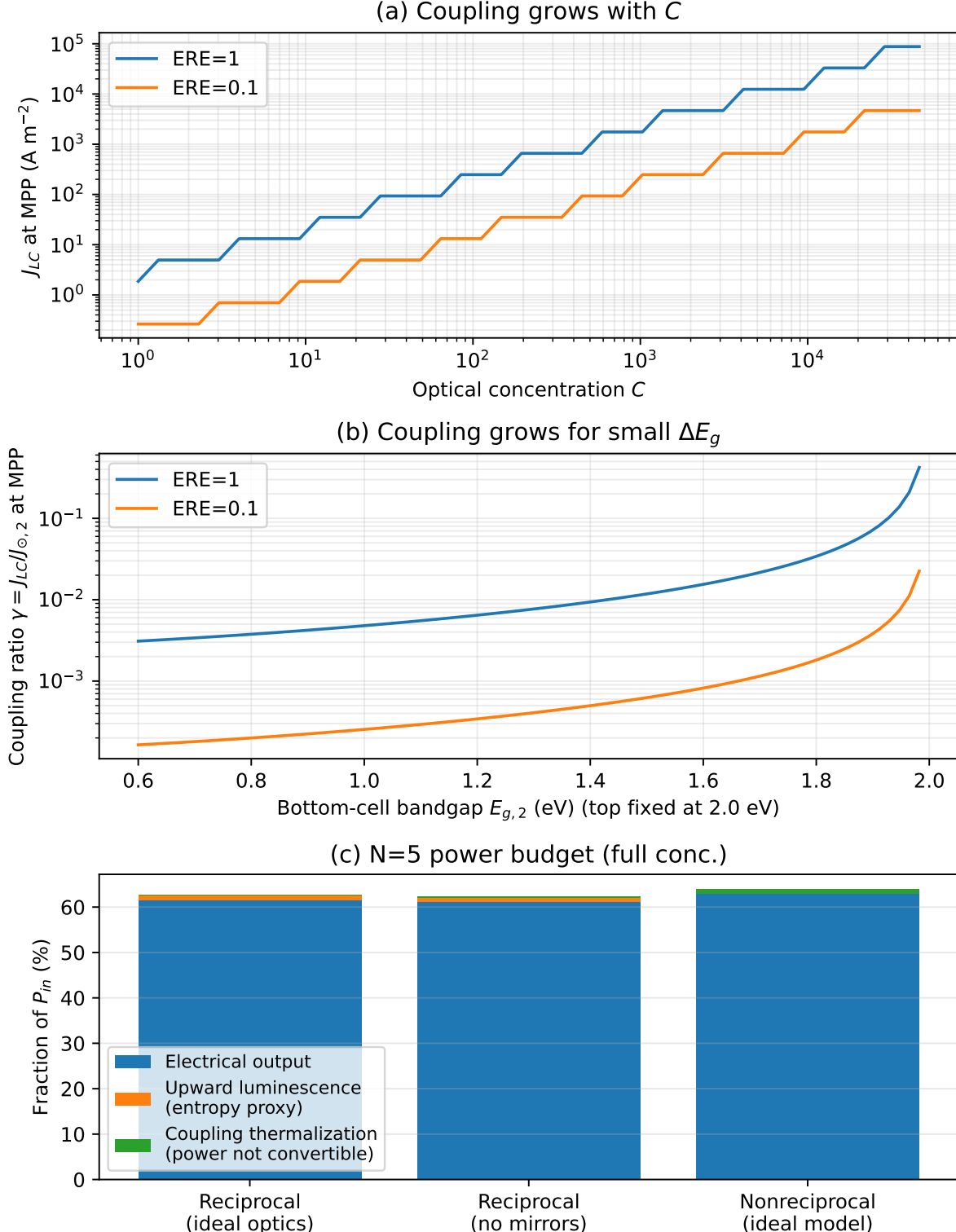


Figure 9: **Luminescent coupling conditions and entropy/thermalization power budget.** (a) Downward luminescent coupling current at MPP increases strongly with optical concentration and is larger for higher ERE. (b) Coupling ratio $\gamma = J_{LC}/J_{\infty,2}$ increases rapidly as the bandgap spacing decreases. (c) Power-budget decomposition for the representative $N = 5$ ladder under full concentration, comparing reciprocal ideal optics (no coupling), reciprocal stacks without intermediate mirrors (two-sided emission + coupling), and an idealized nonreciprocal model. Upward-emitted luminescence is shown as an entropy-loss proxy; coupling thermalization quantifies luminescent power not convertible to electrical work in the lower junctions.

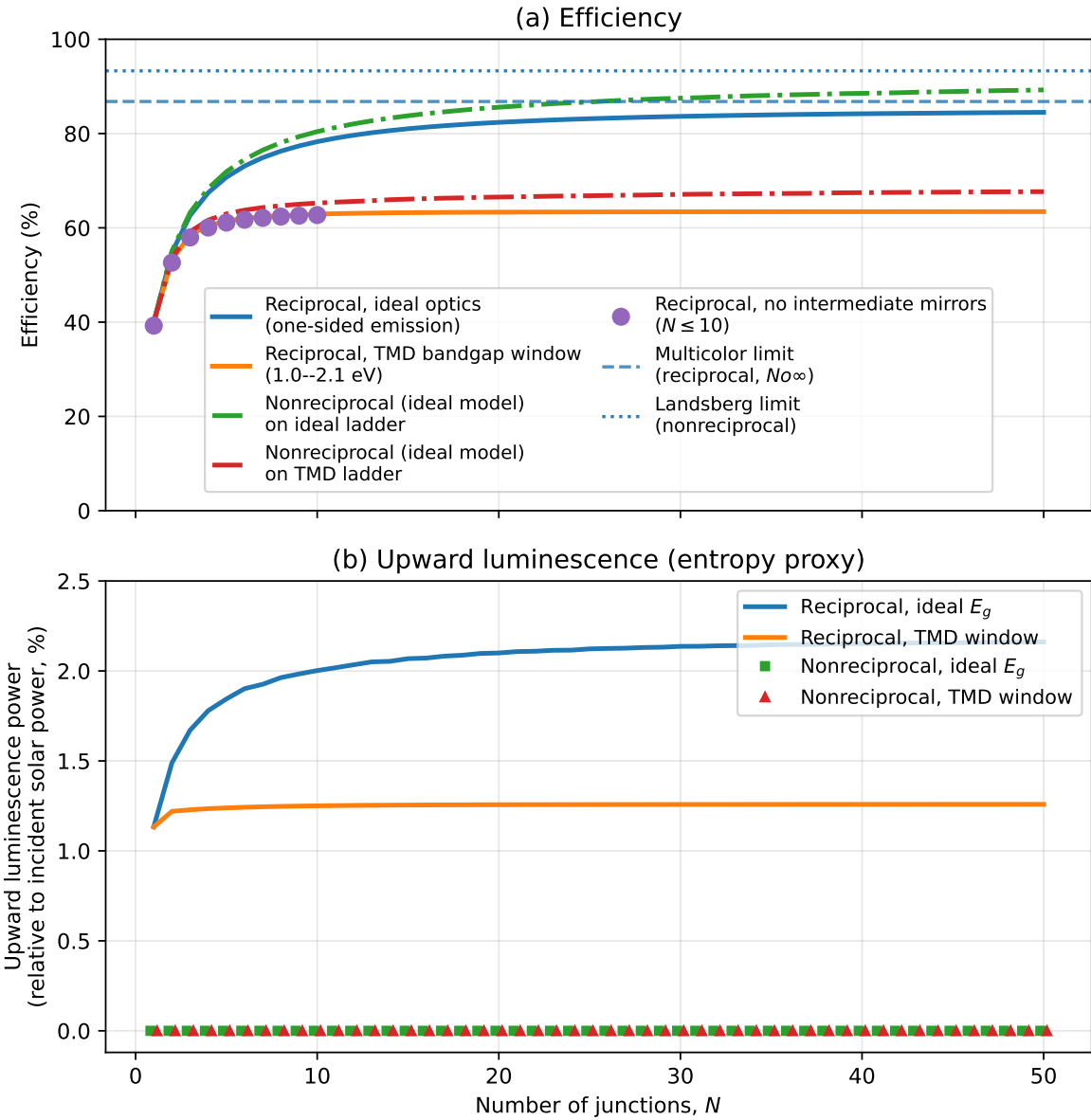
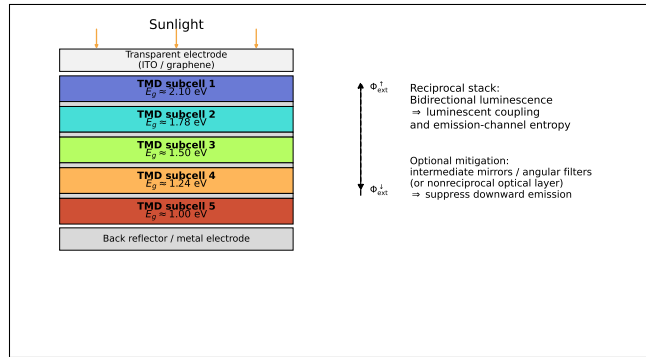


Figure 10: **Reciprocal vs nonreciprocal headroom under full concentration.** (a) Efficiency versus junction number for reciprocal split-spectrum multijunctions (one-sided emission, no coupling), and for the idealized nonreciprocal multijunction model of Fan et al.⁹ applied to the same reciprocity-optimized bandgap ladders (Option A). Filled markers show a reciprocal-stack estimate without intermediate mirrors (two-sided emission + downward luminescent coupling) for $N \leq 10$. (b) Upward-emitted luminescence power fraction $P_{\text{lum}}^{\uparrow}/P_{\text{in}}$ as an entropy-loss proxy. In the idealized nonreciprocal model used here, the upward-emitted luminescence is identically zero, so the nonreciprocal series in (b) are shown with a slight horizontal offset for visibility. Horizontal lines indicate literature multicolor and Landsberg limits for comparison (values depend weakly on T_s).⁹

TOC Graphic



Supporting Information:

Transition Metal Dichalcogenides Multijunction

Solar Cells Toward the Multicolor Limit

Seungwoo Lee*

*Department of Integrated Energy Engineering (College of Engineering) & KU-KIST
Graduate School of Converging Science and Technology, Korea University, Seoul 02841,
Republic of Korea*

E-mail: seungwoo@korea.ac.kr

Supporting Information Overview

This Supporting Information (SI) provides: (i) step-by-step derivations of the detailed-balance equations used in the manuscript; (ii) numerical/algorithmic details for the unlimited-junction bandgap optimization; (iii) explicit definitions of upward-luminescence “entropy-loss proxy” and coupling thermalization bookkeeping; (iv) the excitonic absorptance model and the thickness-dependent reciprocity-consistent calculations; and (v) implementation notes for the reciprocal/no-mirror and ideal nonreciprocal chain model.

Contents

Supporting Information Overview	S-1
1 Constants, geometry, and spectral model	S-5

1.1	Physical constants (SI units)	S-5
1.2	Blackbody photon radiance and solar étendue	S-5
1.3	Full concentration convention	S-6
1.4	Numerical integration range and high-energy cutoff	S-6
2	Single-junction detailed balance: derivations and validation	S-6
2.1	General absorptance form	S-6
2.2	External radiative efficiency (ERE) and total dark current	S-7
2.3	Analytic maximum power point (Lambert- <i>W</i>)	S-7
2.4	Canonical validation checks (order-of-magnitude)	S-8
3	Unlimited-junction split-spectrum multijunction model	S-8
3.1	Window definition and step absorbers	S-8
3.2	Total power and dynamic-programming optimization	S-8
3.3	Practical notes: grid choice and computational complexity	S-9
4	Reciprocity, emission channels, and the role of mirrors	S-9
4.1	Reciprocity relation (Rau 2007)	S-9
4.2	Mirror reflectivity and external luminescence	S-10
5	Luminescent coupling chain model (reciprocal and nonreciprocal)	S-10
5.1	Coupled current equations	S-10
5.2	MPP optimization method (coordinate ascent)	S-11
5.3	Upward luminescence power as an entropy-loss proxy	S-11
5.4	Coupling thermalization bookkeeping	S-11
6	TMD optical response, candidate material library, and excitonic absorptance model	S-12
6.1	Reciprocity-consistent thickness-dependent absorptance	S-12
6.2	Optical-constant conventions: $n(\lambda)$, $k(\lambda)$, and $\alpha(\lambda)$	S-13

6.3	Candidate bandgap library for vdW/TMD absorbers within 1.0–2.1 eV	S-14
6.4	Prioritized mapping to the representative $N = 5$ ladder	S-17
6.5	Minimal excitonic absorption coefficient model	S-18
6.6	Material-specific excitonic parameter suggestions (optional sensitivity sets) . .	S-19
6.7	Additional thickness figures	S-20
7	Nanophotonic bounds and Miller thickness constraints	S-21
7.1	Why introduce a thickness-dependent broadband proxy?	S-21
7.2	Yu–Raman–Fan nanophotonic bounds (2010)	S-21
7.3	Miller “Why optics needs thickness” (2023)	S-22
7.4	Thickness-dependent proxy used in this work	S-22
8	Nonreciprocal multijunction benchmark	S-23
8.1	Ideal nonreciprocal multijunction model	S-23
8.2	No SQ-breaking in single junction	S-23
9	Extended bandgap-ladder tables (reproducibility)	S-23
A1.	Conservative TMD window (full concentration)	S-23
A2.	Unconstrained bandgaps (full concentration)	S-24
A3.	Conservative TMD window (1 sun)	S-24
A4.	Unconstrained bandgaps (1 sun)	S-25
10	Additional figures for the representative $N = 5$ stack	S-25
11	Full ladder lists (text form)	S-27
	Conservative TMD window (full concentration)	S-27
	Unconstrained bandgaps (full concentration)	S-31
	Conservative TMD window (1 sun)	S-36
	Unconstrained bandgaps (1 sun)	S-40

1 Constants, geometry, and spectral model

1.1 Physical constants (SI units)

We use the physical constants summarized in Table S1:

$$q = 1.602176634 \times 10^{-19} \text{ C}, \quad (1)$$

$$h = 6.62607015 \times 10^{-34} \text{ Js}, \quad (2)$$

$$c = 2.99792458 \times 10^8 \text{ m/s}, \quad (3)$$

$$k_B = 1.380649 \times 10^{-23} \text{ J/K}. \quad (4)$$

Table S1: Physical constants used throughout the detailed-balance and reciprocity derivations.

Symbol	Meaning	Value
q	elementary charge	$1.602176634 \times 10^{-19} \text{ C}$
h	Planck constant	$6.62607015 \times 10^{-34} \text{ Js}$
c	speed of light	$2.99792458 \times 10^8 \text{ m/s}$
k_B	Boltzmann constant	$1.380649 \times 10^{-23} \text{ J/K}$

1.2 Blackbody photon radiance and solar étendue

The spectral photon flux per unit area per steradian per unit energy is

$$\Phi_{\text{bb}}(E, T) = \frac{2E^2}{h^3 c^2} \frac{1}{\exp(E/k_B T) - 1}. \quad (5)$$

The sun subtends solid angle $\Omega_s = \pi \sin^2 \theta_s$ with solar half-angle $\theta_s \simeq 0.266^\circ$. Optical concentration is represented by multiplying the incident flux by a factor C :

$$\Phi_{\odot}(E; C) = C \Omega_s \Phi_{\text{bb}}(E, T_s). \quad (6)$$

Throughout, $T_s = 5778\text{ K}$ and $T_c = 300\text{ K}$ unless otherwise noted.

1.3 Full concentration convention

In the classical SQ convention, the maximum concentration corresponds to increasing the effective solar étendue until the incident illumination fills π steradians, giving

$$C_{\max} = \frac{1}{\sin^2 \theta_s} \approx 4.64 \times 10^4. \quad (7)$$

This convention is consistent with the use of a hemispherical emission factor $\Omega_{\text{emit}} = 2\pi$ for one-sided emission in the diode dark current.^{S1,S2}

1.4 Numerical integration range and high-energy cutoff

All integrals are evaluated on an energy grid spanning 0.01 eV to 10 eV. For $T_s = 5778\text{ K}$, the excluded power above 10 eV is negligible, while excluding power above 4.5 eV would omit $\sim 2\%$ of the incident power (see code notes). Using 10 eV therefore improves quantitative agreement with canonical thermodynamic limits without materially affecting computational cost.

2 Single-junction detailed balance: derivations and validation

2.1 General absorptance form

For a device with absorptance $A(E)$, the photogenerated current density is

$$J_{\text{sc}} = q \int_0^\infty A(E) \Phi_{\odot}(E; C) dE. \quad (8)$$

By Kirchhoff's law and reciprocity, the radiative emission spectrum under bias V is

$$\phi_{\text{em}}(E, V) = A(E) \Phi_{\text{bb}}(E, T_c) \Omega_{\text{emit}} (e^{qV/k_B T_c} - 1). \quad (9)$$

Integrating this photon flux yields the radiative recombination current:

$$J_{\text{rad}}(V) = q \int_0^\infty A(E) \Phi_{\text{bb}}(E, T_c) \Omega_{\text{emit}} (e^{qV/k_B T_c} - 1) dE = J_{0,\text{rad}} (e^{qV/k_B T_c} - 1), \quad (10)$$

where

$$J_{0,\text{rad}} = q \int_0^\infty A(E) \Phi_{\text{bb}}(E, T_c) \Omega_{\text{emit}} dE. \quad (11)$$

2.2 External radiative efficiency (ERE) and total dark current

We incorporate nonradiative recombination via

$$J_0 = \frac{J_{0,\text{rad}}}{\text{ERE}}, \quad (12)$$

leading to the ideal-diode equation

$$J(V) = J_{\text{sc}} - J_0 (e^{qV/k_B T_c} - 1). \quad (13)$$

This reproduces the standard SQ triangle voltage penalty $\Delta V = (k_B T_c/q) \ln(\text{ERE})$ and matches the thermodynamic voltage-loss decomposition in Rau et al.^{S3,S4}

2.3 Analytic maximum power point (Lambert- W)

Setting $\partial(VJ)/\partial V = 0$ yields

$$(1 + v)e^v = 1 + \frac{J_{\text{sc}}}{J_0}, \quad v \equiv \frac{qV}{k_B T_c}, \quad (14)$$

so

$$v_{\text{mpp}} = W\left(e\left[1 + \frac{J_{\text{sc}}}{J_0}\right]\right) - 1, \quad V_{\text{mpp}} = \frac{k_B T_c}{q} v_{\text{mpp}}. \quad (15)$$

The corresponding J_{mpp} and P_{mpp} follow directly.

2.4 Canonical validation checks (order-of-magnitude)

Using the blackbody solar model and $A(E) = \Theta(E - E_g)$ with one-sided emission ($\Omega_{\text{emit}} = 2\pi$), the code reproduces canonical SQ-like trends: (i) full concentration increases V_{oc} and η relative to 1 sun, (ii) the optimal E_g shifts downward with increasing concentration, and (iii) V_{oc} and η penalize logarithmically with reduced ERE. Absolute values differ modestly from AM1.5G SQ limits because of the blackbody spectrum and geometric conventions.

3 Unlimited-junction split-spectrum multijunction model

3.1 Window definition and step absorbers

We define descending bandgaps $E_{g,1} > E_{g,2} > \dots > E_{g,N}$ and adopt split-spectrum windows

$$E \in [E_{g,i}, E_{g,i-1}), \quad E_{g,0} \equiv E_{\text{max}}. \quad (16)$$

For step absorbers, $A_i(E) = 1$ within the window and 0 outside. Generation and radiative recombination are restricted to the same window, which is consistent with ideal spectral splitting optics (filters) that enforce identical acceptance for absorption and emission (reciprocity).

3.2 Total power and dynamic-programming optimization

The total maximum power is

$$P_{\text{tot}}^* = \sum_{i=1}^N P_i^*(E_{g,i}; E_{g,i-1}), \quad (17)$$

where each term is obtained from the single-junction analytic MPP in Section 2. Discretizing E_g on a grid $\{E^{(k)}\}$, define $P^*(E^{(k)}, E^{(j)})$ for $j > k$ and use

$$F(n, k) = \max_{j > k} [F(n - 1, j) + P^*(E^{(k)}, E^{(j)})], \quad (18)$$

with $F(1, k) = P^*(E^{(k)}, E_{\max})$. Backtracking yields the optimal ladder.

3.3 Practical notes: grid choice and computational complexity

If the grid size is K , precomputing P^* requires $\mathcal{O}(K^2)$ evaluations. The DP recurrence requires $\mathcal{O}(NK^2)$ operations. For the conservative TMD window (1.0–2.1 eV with 0.01 eV spacing; $K \approx 111$) and $N \leq 50$, this is computationally light (seconds on a laptop). For the unconstrained case we use a coarser grid (0.02 eV spacing) to balance accuracy and cost; the SI code allows refinement.

4 Reciprocity, emission channels, and the role of mirrors

4.1 Reciprocity relation (Rau 2007)

Rau derived that the emitted electroluminescence spectrum is directly related to the external quantum efficiency (EQE) under reciprocity.^{S5} In our notation, using absorptance $A(E)$ as the reciprocity-relevant optical response,

$$\phi_{\text{em}}(E, V) \propto A(E) \Phi_{\text{bb}}(E, T_c) (e^{qV/k_B T_c} - 1). \quad (19)$$

Thus any thickness- or nanophotonic modification of $A(E)$ changes both the generation and the radiative emission channels.

4.2 Mirror reflectivity and external luminescence

Miller and Yablonovitch emphasized that approaching SQ requires strong external luminescence and that back-mirror reflectivity can be crucial for photon recycling and extraction.^{S6} In our framework, a perfect back reflector changes Ω_{emit} from 4π to 2π (one-sided emission), reducing $J_{0,\text{rad}}$ by a factor of two and increasing V by $(k_B T_c/q) \ln 2$. In multijunction stacks, analogous emission-channel control is typically achieved by intermediate mirrors or angular filters between subcells.

5 Luminescent coupling chain model (reciprocal and nonreciprocal)

5.1 Coupled current equations

For junction i , define upward/downward hemispherical radiative prefactors

$$J_{0,i}^{\uparrow/\downarrow} = q \int_{E_{g,i}}^{E_{g,i-1}} A_i(E) \Phi_{\text{bb}}(E, T_c) (2\pi) dE. \quad (20)$$

Then

$$J_{\text{rad},i}^{\uparrow/\downarrow}(V_i) = J_{0,i}^{\uparrow/\downarrow} (e^{qV_i/k_B T_c} - 1). \quad (21)$$

Assuming full absorption of downward photons by junction $i + 1$, the current becomes

$$J_i(V_i) = J_{\odot,i} + J_{\text{rad},i-1}^{\downarrow}(V_{i-1}) - \frac{J_{0,i}^{\uparrow} + J_{0,i}^{\downarrow}}{\text{ERE}_i} (e^{qV_i/k_B T_c} - 1), \quad (22)$$

with $J_{\text{rad},0}^{\downarrow} \equiv 0$. The system output is

$$P = \sum_{i=1}^N V_i J_i(V_i), \quad (23)$$

maximized over $\{V_i\}$.

5.2 MPP optimization method (coordinate ascent)

We maximize $P(\{V_i\})$ by coordinate ascent: iteratively sweep each V_i over a grid $[0, E_{g,i}]$ while holding other voltages fixed. Because coupling is unidirectional in this model, each V_i primarily affects J_i and J_{i+1} , and convergence is typically rapid for $N \leq 50$. We also provide hooks to replace coordinate ascent with gradient-free optimizers if desired.

5.3 Upward luminescence power as an entropy-loss proxy

We define the upward emitted luminescence power

$$P_{\text{lum}}^{\uparrow} = \sum_i \int_{E_{g,i}}^{E_{g,i-1}} E A_i(E) \Phi_{\text{bb}}(E, T_c) (2\pi) (e^{qV_i/k_B T_c} - 1) dE, \quad (24)$$

and report $P_{\text{lum}}^{\uparrow}/P_{\text{in}}$.

5.4 Coupling thermalization bookkeeping

The downward luminescence power emitted by junction i is

$$P_{\text{lum},i}^{\downarrow} = \int_{E_{g,i}}^{E_{g,i-1}} E A_i(E) \Phi_{\text{bb}}(E, T_c) (2\pi) (e^{qV_i/k_B T_c} - 1) dE. \quad (25)$$

Assuming one electron generated per absorbed photon in junction $i+1$ and extracted at V_{i+1} , the electrical work extracted from the coupling current $J_{\text{LC},i} = J_{\text{rad},i}^{\downarrow}$ is $V_{i+1} J_{\text{LC},i}$. We define coupling thermalization proxy

$$P_{\text{therm}}^{\text{LC}} = \sum_{i=1}^{N-1} (P_{\text{lum},i}^{\downarrow} - V_{i+1} J_{\text{LC},i}). \quad (26)$$

This explicitly separates upward entropy loss from the (partially recoverable) energy transferred downward.

6 TMD optical response, candidate material library, and excitonic absorptance model

6.1 Reciprocity-consistent thickness-dependent absorptance

For each junction we use a thickness-dependent absorptance written in Beer–Lambert form,

$$A(E; t) = 1 - \exp[-\alpha(E) F(E) t], \quad (27)$$

where t is the absorber thickness, $\alpha(E)$ is the intrinsic absorption coefficient, and $F(E)$ is a dimensionless optical path-length enhancement factor. At an elementary level, $F(E) = L_{\text{eff}}(E)/t$ is the ratio between the average optical path length experienced by photons inside the absorber and the physical thickness: $F(E) = 1$ corresponds to a single-pass planar film, while $F(E) > 1$ captures multi-pass propagation and light trapping (back reflectors, resonant cavities, scattering/angle randomization, etc.).

Key point (reciprocity): the same $A(E; t)$ must be used in both the generation term (J_{sc}) and the radiative dark current ($J_{0,\text{rad}}$) to enforce reciprocity.^{S5} This reciprocity-consistent treatment is essential when discussing voltage losses and luminescence thermodynamics, because any optical design that increases absorption in a given spectral window must also increase emission in that same window.

Broadband nanophotonic proxy used in this work. In realistic ultrathin TMD stacks, the achievable enhancement is thickness-limited: the geometric-optics Yablonovitch bound $F \leq 4n^2$ can only be approached when the absorber is optically thick enough to support many radiative/guided channels (see Section 7). To map these ideas into a compact detailed-balance model, we introduce a normalized broadband enhancement function $g(t) \in [0, 1]$ and

define a thickness-dependent effective enhancement factor

$$F_{\text{proxy}}(t) = 1 + (4n^2 - 1) g(t). \quad (28)$$

In our calculations we approximate $F(E) \approx F_{\text{proxy}}(t)$, i.e., we use a wavelength-independent enhancement as a broadband average. We adopt the simple saturating form $g(t) = 1 - \exp(-t/t_0)$ with $t_0 = 200$ nm, and use $n = 4.5$ as a representative TMD index for the $4n^2$ limit (Section 7). This “proxy” is not meant to replace full wave-optics modeling for a specific architecture; rather, it provides an elementary, physically motivated way to translate nanophotonic bounds into thickness requirements in detailed-balance calculations.

6.2 Optical-constant conventions: $n(\lambda)$, $k(\lambda)$, and $\alpha(\lambda)$

We describe optical response using the complex refractive index

$$\tilde{n}(E) = n(E) + i k(E), \quad (29)$$

where n is the refractive index and k is the extinction coefficient. The absorption coefficient α (in m^{-1}) and k are related by^{S7}

$$\alpha(\lambda) = \frac{4\pi k(\lambda)}{\lambda} \quad \Leftrightarrow \quad k(\lambda) = \frac{\alpha(\lambda)\lambda}{4\pi}. \quad (30)$$

Writing $\lambda = hc/E$ yields the equivalent energy-domain relation (used in our code when E is expressed in joules):^{S8}

$$\alpha(E) = \frac{4\pi k(E)E}{hc}. \quad (31)$$

These relations enable consistent bookkeeping between (i) empirical optical-constant datasets reported as $k(E)$ and (ii) absorption models parameterized directly in terms of $\alpha(E)$.

Representative n values. In the detailed-balance calculations, the optical constants

enter in two ways: (i) via the absorptance $A(E; t)$ (through α) and (ii) via nanophotonic/path-length enhancement proxies that depend on n (e.g., the geometric-optics factor $4n^2$). Reich et al. (Pop group) report representative refractive indices n at the bandgap energy for several bulk group-VI TMDs.^{S8} Table S2 reproduces these representative values for convenient reference.

Table S2: Representative refractive index values at the bandgap energy for selected bulk TMDs (from Ref.^{S8}).

Material (bulk)	E_g (eV)	$n(E_g)$	Notes
MoS ₂	1.29	4.48	indirect gap (bulk)
MoSe ₂	1.09	4.79	indirect gap (bulk)
WS ₂	1.38	4.17	indirect gap (bulk)
WSe ₂	1.20	4.70	indirect gap (bulk)

Working refractive index. Unless otherwise stated, we use a representative constant index $n = 4.5$ in the nanophotonic proxy calculations (Figure 8) and in the broadband path-length enhancement proxy $F(E)$, consistent with Table S2. The thickness-dependent detailed-balance results are primarily controlled by $\alpha(E)$ rather than weak dispersion of $n(E)$; including full dispersion is straightforward in the provided code by replacing n with tabulated $n(E)$ and using a transfer-matrix method (TMM) for multilayers.

6.3 Candidate bandgap library for vdW/TMD absorbers within 1.0–2.1 eV

Table S3 compiles representative optical-gap ranges for a subset of vdW semiconductors relevant to the conservative 1.0–2.1 eV window used in the manuscript (Option A). Values depend on thickness (direct↔indirect transitions), dielectric environment, strain, and alloying; the table is intended as a design map rather than a definitive database.^{S8–S10}

Table S3: Candidate vdW/TMD absorber library within the conservative 1.0–2.1 eV optical-gap window. “1L” denotes monolayer; “few-L” denotes few-layer. Reported gaps are representative optical-transition energies; actual values depend on thickness, dielectric screening, strain, and temperature.^{S8–S10}

Material family	Variant / tuning knob	$E_{g,\text{opt}}$ (eV)	Notes / design relevance
Group-VI TMDs	WS ₂ (1L)	~2.0–2.1	Wide-gap visible absorber; strong A/B excitons; good candidate for ~2.1 eV top rung.
Group-VI TMDs	MoS ₂ (1L)	~1.8–1.95	Strong visible absorption; canonical monolayer TMD; candidate for ~1.8 eV rung.
Group-VI TMDs	WSe ₂ (1L)	~1.6–1.7	Red/near-IR edge for monolayer; thickness-tunable; candidate for mid rungs.
Group-VI TMDs	MoSe ₂ (1L)	~1.5–1.6	Mid-gap monolayer; strong excitons; candidate for ~1.5 eV rung.
Group-VI TMDs	MoTe ₂ (few-L/bulk)	~0.95–1.1	Narrow-gap within conservative window; candidate for ~1.0 eV bottom rung (encapsulation needed).
Group-VI TMDs	WS ₂ (2L–few-L)	~1.6–1.9	Thickness reduces gap; candidate for ~1.7–1.8 eV rung if monolayer gap is too high.
Group-VI TMDs	MoS ₂ (bulk)	~1.2–1.3	Indirect gap; useful for ~1.24 eV rung with increased thickness to compensate absorptance.

Continued on next page

Material family	Variant / tuning knob	$E_{g,\text{opt}}$ (eV)	Notes / design relevance
Group-VI TMDs	WSe ₂ (few-L/bulk)	~1.2–1.4	Thickness-tunable; candidate for ~1.24 eV rung; indirectness may reduce radiative efficiency unless photon recycling is strong.
Group-VI TMDs	MoSe ₂ (bulk)	~1.1–1.2	Candidate near ~1.1 eV; could serve as alternate bottom rung if MoTe ₂ is unavailable.
Alloyed TMDs	MoS _{2(1-x)} Se _{2x}	~1.55–1.9	Alloying provides quasi-continuous tuning between MoS ₂ and MoSe ₂ ; can “fill” ladder gaps.
Alloyed TMDs	WS _{2(1-x)} Se _{2x}	~1.6–2.1	Tunable wide-gap branch; candidates for top/mid rungs while retaining strong excitons.
Re-based TMDs	ReS ₂ (few-L)	~1.45–1.6	In-plane anisotropic; often retains a direct-like optical transition across thickness; candidate near ~1.5 eV rung.
Re-based TMDs	ReSe ₂ (few-L)	~1.25–1.45	Candidate for ~1.24 eV rung; anisotropic optics may be leveraged for polarization-selective trapping.
Other layered chalcogenides	SnSe ₂ (few-L)	~1.0–1.2	Layered semiconductor; potential bottom-rung alternative; optical constants and contacts need evaluation.

Continued on next page

Material family	Variant / tuning knob	$E_{g,\text{opt}}$ (eV)	Notes / design relevance
Other layered chalcogenides	InSe (few-L)	~1.2–1.6	High mobility vdW semiconductor; candidate for ~1.24 eV rung and above; often used in heterostructures.
Other layered chalcogenides	GaSe (few-L)	~1.8–2.1	Wide-gap layered chalcogenide; possible alternative for top rung if TMD options are limited.
Black phosphorus	BP (thickness-tuned, encapsulated)	~0.3–2.0	Broadly tunable by thickness; environmental instability requires encapsulation; could “bridge” gaps but is not a TMD.

6.4 Prioritized mapping to the representative $N = 5$ ladder

The DP-optimized conservative-window ladder for $N = 5$ is (top→bottom)

$$(2.10, 1.78, 1.50, 1.24, 1.00) \text{ eV.} \quad (32)$$

Table S4 summarizes one pragmatic rung-to-material mapping consistent with the conservative window and the transfer-printing motivation of the manuscript. We emphasize that the “best” mapping is application-specific and should consider ERE, achievable thickness, contact selectivity, and stability (encapsulation). The broader candidate library in Table S3 can be used to generate alternative stacks.

Table S4: Prioritized mapping of realistic vdW/TMD candidates to the representative $N = 5$ target bandgap ladder (Option A). “Primary” emphasizes group-VI TMDs; “alternates” illustrate thickness/alloy/other-vdW routes.

Target E_g (eV)	Primary	Alternates	Practical notes
2.10	WS ₂ (1L)	GaSe (few-L); WS _{2(1-x)} Se _{2x} (alloy)	Top cell benefits strongly from high ERE because its voltage loss propagates through the stack power sum.
1.78	MoS ₂ (1L)	WS ₂ (2L-few-L); MoS _{2(1-x)} Se _{2x}	Contact resistance and optical parasitics at the top interface dominate because currents are largest in upper cells.
1.50	MoSe ₂ (1L)	ReS ₂ ; WSe ₂ (1L, strain)	Mid-gap rung is often easiest to realize with monolayers; exciton linewidth and outcoupling set ERE.
1.24	WSe ₂ (few-L/bulk)	MoS ₂ (bulk); InSe (few-L); ReSe ₂	For indirect multilayers, thickness and photon recycling (mirrors) become central to maintain voltage.
1.00	MoTe ₂ (few-L/bulk)	SnSe ₂ (few-L); MoSe ₂ (bulk, ~ 1.1)	Bottom rung is the primary limiter in the conservative window; stability and selective contacts are critical.

6.5 Minimal excitonic absorption coefficient model

To capture a TMD-like spectral shape (strong A/B excitons superimposed on a continuum), we use

$$\alpha(E) = \alpha_U(E) + \alpha_{\text{cont}}(E) + \alpha_A(E) + \alpha_B(E), \quad (33)$$

with

$$\alpha_U(E) = \alpha_{U,0} \exp\left(\frac{E - E_g}{E_U}\right) \Theta(E_g - E), \quad (34)$$

$$\alpha_{\text{cont}}(E) = \alpha_{c,0} \left[1 - \exp\left(-\frac{E - E_g}{E_s}\right) \right] \Theta(E - E_g), \quad (35)$$

$$\alpha_{A/B}(E) = A_{A/B} \frac{\Gamma_{A/B}^2}{(E - E_{A/B})^2 + \Gamma_{A/B}^2}, \quad (36)$$

where $E_A = E_g$ and $E_B = E_g + \Delta_B$. Equation (33) is not intended to capture all excitonic fine structure; rather, it provides a compact parameterization that reproduces (i) a sharp excitonic onset, (ii) a broad continuum rise, and (iii) a second higher-energy exciton, consistent with

typical 2D-TMD optical spectra.^{S9,S10}

From the perspective of thickness requirements, it is useful to note that the excitonic Lorentzians provide large $\alpha(E)$ only over a relatively narrow energy range near the band edge. In contrast, the solar spectrum supplies a broad distribution of above-gap photons, and the approach to unity absorptance in an ultrathin film is often controlled by the continuum term $\alpha_{\text{cont}}(E)$ and by the effective optical path length $F(E)t$. As a result, incomplete *broadband* absorption can persist even when the band-edge exciton is strong, leading to substantial transmission losses at small t (main text, Figure 7) and motivating broadband light trapping through $F_{\text{proxy}}(t)$ (Eq. 28 and Section 7).

Table S5: Generic parameter values for the excitonic absorption coefficient model (used for the thickness-dependent examples in this work unless otherwise stated).

Parameter	Symbol	Value
Continuum prefactor	$\alpha_{c,0}$	$1.5 \times 10^7 \text{ m}^{-1}$
Continuum rise scale	E_s	0.25 eV
Continuum saturation	α_{max}	$2.0 \times 10^8 \text{ m}^{-1}$
Urbach prefactor	$\alpha_{U,0}$	$1.0 \times 10^5 \text{ m}^{-1}$
Urbach energy	E_U	0.03 eV
A-exciton amplitude	A_A	$1.0 \times 10^8 \text{ m}^{-1}$
A-exciton width	Γ_A	0.03 eV
B-exciton amplitude	A_B	$0.6 \times 10^8 \text{ m}^{-1}$
B-exciton width	Γ_B	0.04 eV
A–B splitting	Δ_B	0.18 eV

6.6 Material-specific excitonic parameter suggestions (optional sensitivity sets)

Group-VI TMDs exhibit material-dependent A–B exciton splittings (driven by spin–orbit coupling) and linewidths that depend on temperature and disorder. Table S6 provides representative values that can be substituted into Eq. (33) for sensitivity analysis. In the figures presented in this work, unless explicitly indicated, we use the generic set in Table S5 and shift E_g to each rung.

Table S6: Illustrative material-specific excitonic parameters for sensitivity analysis (to be used with Eq. (33)). Values are representative and may vary with temperature, dielectric environment, and thickness.^{S9,S10}

Material	E_A (eV)	Δ_B (eV)	Γ_A (eV)	Γ_B (eV)	Notes
MoS ₂	1.88	0.15–0.20	0.03–0.05	0.04–0.06	Mo-based: smaller spin–orbit splitting
WS ₂	2.05	0.30–0.45	0.03–0.05	0.04–0.07	W-based: larger splitting; strong visible excitons
MoSe ₂	1.55	0.18–0.25	0.03–0.06	0.04–0.07	Candidate for \sim 1.5 eV rung
WSe ₂	1.65	0.35–0.50	0.03–0.06	0.04–0.08	Candidate for mid/near-IR rungs
MoTe ₂	1.05	0.15–0.25	0.03–0.07	0.04–0.09	Narrow-gap; encapsulation typically required

6.7 Additional thickness figures

For convenience, Figure S1 reproduces the layer-resolved thickness trends referenced in the main text.

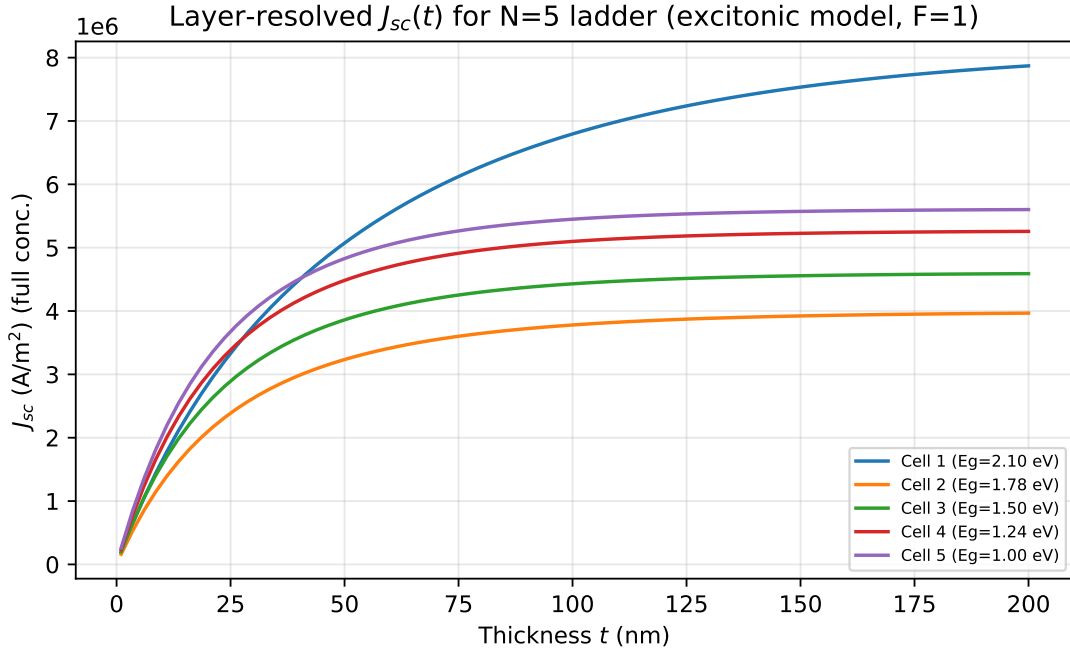


Figure S1: Layer-resolved $J_{sc}(t)$ for the representative $N = 5$ ladder (excitonic model, single-pass).

7 Nanophotonic bounds and Miller thickness constraints

7.1 Why introduce a thickness-dependent broadband proxy?

The detailed-balance framework requires a model for how efficiently each subcell absorbs above-gap sunlight. For an optically thin film, the Beer–Lambert form $A(E; t) = 1 - \exp[-\alpha(E)F(E)t]$ is a convenient way to connect microscopic material absorption (α) to a macroscopic device response. The dimensionless factor $F(E)$ summarizes optical design: it increases the effective photon dwell time (or average path length) inside the absorber relative to a single-pass film. In the geometric-optics limit, where ray directions can be randomized many times before escape, the broadband average enhancement is bounded by the well-known Yablonovitch limit $F \leq 4n^2$. However, when the absorber thickness approaches the wavelength ($t \lesssim \lambda$), the number of radiative and guided modes that can participate is limited, and the enhancement that can be sustained *over a broad spectrum* is reduced. This is the motivation for introducing a thickness-dependent broadband proxy (the normalized function $g(t)$ and the corresponding $F_{\text{proxy}}(t)$ used in the main text and in the thickness sweeps of Figure 7).

7.2 Yu–Raman–Fan nanophotonic bounds (2010)

Yu, Raman, and Fan derived wave-optics bounds on absorption enhancement in nanophotonic structures as a function of thickness and in-plane periodicity, showing that the geometric-optics Lambertian $4n^2$ limit is not universally applicable in ultrathin films.^{S11} The key qualitative message is that wavelength-scale textures support a *discrete* set of optical channels; strong enhancement is possible, but it is often resonant and therefore narrowband, while maintaining large enhancement across a broad bandwidth generally requires larger thickness (more modes and more channels).

7.3 Miller “Why optics needs thickness” (2023)

Miller emphasized a related and more general viewpoint: many broadband optical functionalities intrinsically require finite thickness because the number of independently controllable channels (degrees of freedom) scales with thickness.^{S12} In the context of ultrathin multijunction absorbers, this reinforces that there is an unavoidable trade-off between extreme thickness reduction and broadband optical performance, even before considering practical issues such as contact losses, series resistance, or parasitic absorption.

7.4 Thickness-dependent proxy used in this work

To keep the detailed-balance model analytically transparent, we translate the above thickness-limited trend into a simple scalar proxy. We define a normalized enhancement function $g(t) \in [0, 1]$ and construct

$$F_{\text{proxy}}(t) = 1 + (4n^2 - 1) g(t), \quad (37)$$

so that $F_{\text{proxy}}(t) = 1$ for a single pass and $F_{\text{proxy}}(t) \rightarrow 4n^2$ only in the thick limit. In the calculations reported here we take $n = 4.5$ as a representative TMD index and use the saturating form $g(t) = 1 - \exp(-t/t_0)$ with $t_0 = 200$ nm; the resulting $g(t)$ curve is plotted in Figure 8c of the main text. This proxy is not intended to be a rigorous upper bound; rather, it provides an elementary, physically motivated way to explore how thickness constraints and broadband light trapping translate into multijunction performance metrics. More architecture-specific modeling can be performed by replacing $g(t)$ (or $F(E)$) with a wavelength-dependent function computed from electromagnetic simulations or from published nanophotonic bounds.

8 Nonreciprocal multijunction benchmark

8.1 Ideal nonreciprocal multijunction model

We implement an idealized nonreciprocal chain by suppressing upward emission ($J_{0,i}^\uparrow = 0$) while retaining downward emission and full absorption in the next junction.^{S13} This suppresses upward luminescence power (entropy-loss proxy) and provides additional headroom in multijunction architectures.

8.2 No SQ-breaking in single junction

Fan and co-workers showed that nonreciprocity does not break the SQ limit for single-junction solar cells under detailed balance.^{S14} Accordingly, in our comparisons we treat the $N = 1$ case as having no nonreciprocal gain, while $N > 1$ can benefit.

9 Extended bandgap-ladder tables (reproducibility)

The following tables list DP-optimized bandgap ladders and efficiencies used throughout this paper (Tables S7–S10). For convenience, we also cite them individually below as Tables S7, S8, S9, and S10.

A1. Conservative TMD window (full concentration)

Table S7: Optimal TMD-window bandgap ladders (full concentration, ERE=1, split-spectrum). Bandgaps listed top-to-bottom.

N	η (%)	E_g ladder (eV; top→bottom)
1	39.97	1.07
2	53.25	1.85, 1.00
3	58.47	2.10, 1.48, 1.00
4	60.48	2.10, 1.68, 1.32, 1.00
5	61.46	2.10, 1.78, 1.50, 1.24, 1.00

N	η (%)	E_g ladder (eV; top→bottom)
6	62.02	2.10, 1.84, 1.61, 1.39, 1.19, 1.00
7	62.38	2.10, 1.88, 1.68, 1.50, 1.33, 1.16, 1.00
8	62.62	2.10, 1.91, 1.74, 1.58, 1.43, 1.28, 1.14, 1.00
9	62.79	2.10, 1.94, 1.79, 1.64, 1.50, 1.37, 1.24, 1.12, 1.00
10	62.91	2.10, 1.96, 1.82, 1.69, 1.57, 1.45, 1.33, 1.22, 1.11, 1.00

A2. Unconstrained bandgaps (full concentration)

Table S8: Optimal unconstrained bandgap ladders (full concentration, ERE=1, split-spectrum).

N	η (%)	E_g ladder (eV; top→bottom)
1	39.97	1.07
2	54.79	1.65, 0.75
3	62.62	2.03, 1.21, 0.59
4	67.46	2.33, 1.55, 0.99, 0.49
5	70.74	2.55, 1.81, 1.29, 0.85, 0.43
6	73.11	2.77, 2.05, 1.55, 1.13, 0.75, 0.37
7	74.89	2.95, 2.23, 1.75, 1.35, 1.01, 0.69, 0.35
8	76.27	3.09, 2.39, 1.91, 1.53, 1.21, 0.91, 0.61, 0.31
9	77.38	3.23, 2.53, 2.07, 1.69, 1.37, 1.09, 0.83, 0.57, 0.29
10	78.28	3.35, 2.67, 2.21, 1.85, 1.55, 1.27, 1.01, 0.77, 0.53, 0.27

A3. Conservative TMD window (1 sun)

Table S9: Optimal TMD-window bandgap ladders (1 sun, ERE=1, split-spectrum).

N	η (%)	E_g ladder (eV; top→bottom)
1	29.92	1.28
2	41.43	1.85, 1.00
3	46.61	2.10, 1.49, 1.00
4	48.61	2.10, 1.68, 1.32, 1.00
5	49.58	2.10, 1.78, 1.50, 1.24, 1.00

N	η (%)	E_g ladder (eV; top→bottom)
6	50.15	2.10, 1.84, 1.61, 1.39, 1.19, 1.00
7	50.50	2.10, 1.88, 1.68, 1.50, 1.33, 1.16, 1.00
8	50.74	2.10, 1.91, 1.74, 1.58, 1.43, 1.28, 1.14, 1.00
9	50.91	2.10, 1.94, 1.79, 1.64, 1.50, 1.37, 1.24, 1.12, 1.00
10	51.03	2.10, 1.96, 1.82, 1.69, 1.57, 1.45, 1.33, 1.22, 1.11, 1.00

A4. Unconstrained bandgaps (1 sun)

Table S10: Optimal unconstrained bandgap ladders (1 sun, ERE=1, split-spectrum).

N	η (%)	E_g ladder (eV; top→bottom)
1	29.92	1.27
2	41.46	1.83, 0.97
3	47.66	2.19, 1.39, 0.81
4	51.53	2.49, 1.73, 1.19, 0.73
5	54.18	2.71, 1.97, 1.47, 1.05, 0.65
6	56.10	2.91, 2.19, 1.71, 1.31, 0.95, 0.61
7	57.55	3.07, 2.37, 1.89, 1.51, 1.17, 0.87, 0.57
8	58.68	3.23, 2.53, 2.07, 1.71, 1.39, 1.11, 0.83, 0.55
9	59.59	3.35, 2.67, 2.21, 1.85, 1.55, 1.27, 1.01, 0.77, 0.53
10	60.32	3.49, 2.81, 2.35, 1.99, 1.69, 1.43, 1.19, 0.97, 0.75, 0.51

10 Additional figures for the representative $N = 5$ stack

Figure S2 reports layer-resolved operating metrics for the representative $N = 5$ ladder under full concentration, highlighting the joint influence of finite absorptance and external radiative efficiency (ERE) on each subcell's J_{sc} , V_{oc} , and fill factor.

Subcell metrics for N=5 ladder (step absorber, full concentration)

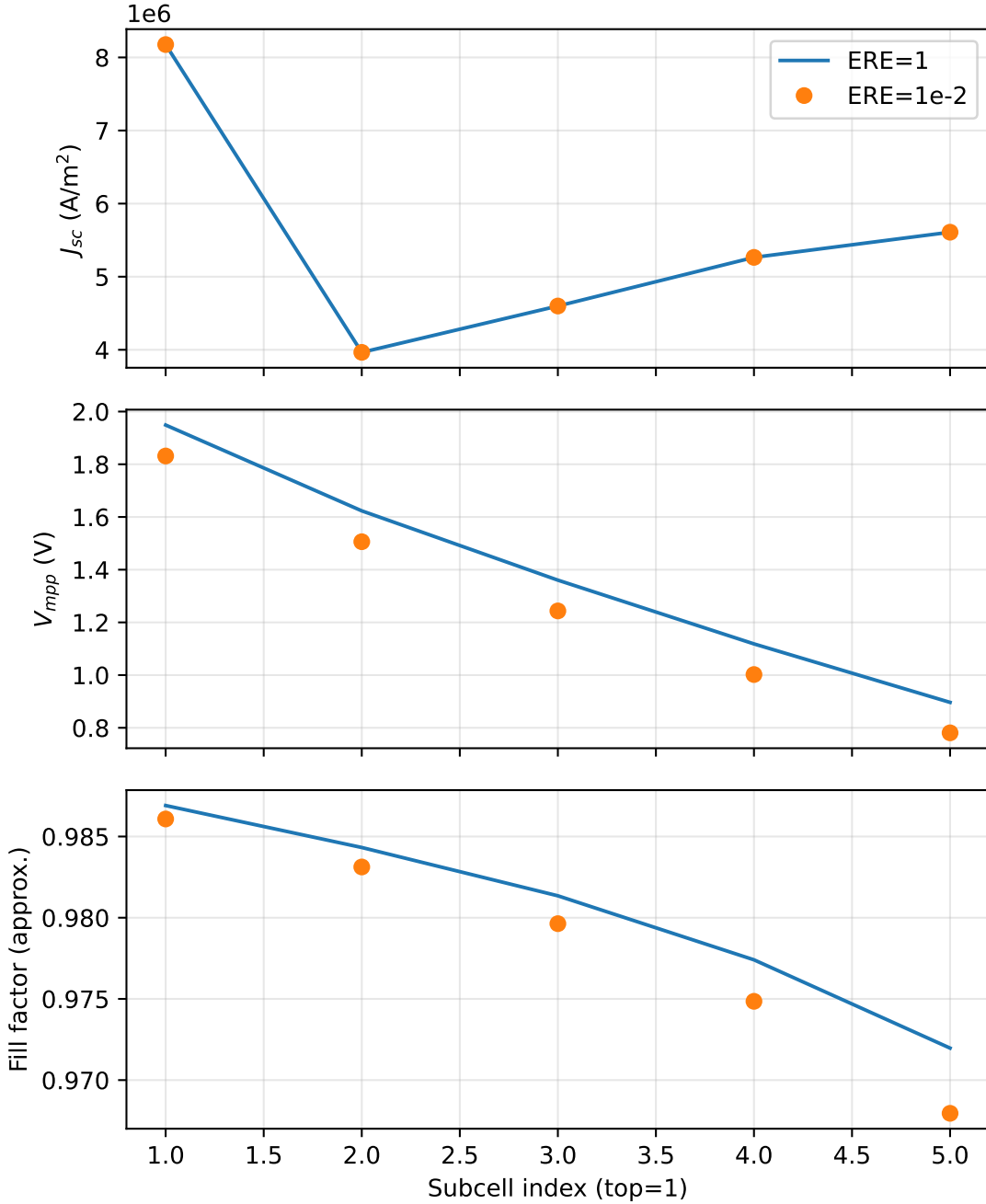


Figure S2: **Subcell operating metrics for the representative $N = 5$ ladder under full concentration (step-absorber model).** Shown are J_{sc} , V_{mpp} , and fill factor (approx.) for ERE = 1 and ERE = 10^{-2} . The two J_{sc} traces overlap (and therefore visually appear as a single curve) because ERE affects the radiative recombination current that sets voltage, but does not change the optical-generation term in the detailed-balance model.

11 Full ladder lists (text form)

For completeness and reproducibility, we list the DP-optimized ladders (top→bottom) for $N = 1 \dots 50$.

Conservative TMD window (full concentration)

```
N= 1: 1.07
N= 2: 1.85, 1.00
N= 3: 2.10, 1.48, 1.00
N= 4: 2.10, 1.68, 1.32, 1.00
N= 5: 2.10, 1.78, 1.50, 1.24, 1.00
N= 6: 2.10, 1.84, 1.61, 1.39, 1.19, 1.00
N= 7: 2.10, 1.88, 1.68, 1.50, 1.33, 1.16, 1.00
N= 8: 2.10, 1.91, 1.74, 1.58, 1.43, 1.28, 1.14, 1.00
N= 9: 2.10, 1.94, 1.79, 1.64, 1.50, 1.37, 1.24, 1.12, 1.00
N=10: 2.10, 1.96, 1.82, 1.69, 1.57, 1.45, 1.33, 1.22, 1.11, 1.00
N=11: 2.10, 1.97, 1.85, 1.73, 1.62, 1.51, 1.40, 1.30, 1.20, 1.10, 1.00
N=12: 2.10, 1.98, 1.87, 1.76, 1.66, 1.56, 1.46, 1.36, 1.27, 1.18, 1.09, 1.00
N=13: 2.10, 1.99, 1.89, 1.79, 1.69, 1.60, 1.51, 1.42, 1.33, 1.24, 1.16, 1.08,
      1.00
N=14: 2.10, 2.00, 1.90, 1.81, 1.72, 1.63, 1.55, 1.47, 1.39, 1.31, 1.23, 1.15,
      1.07, 1.00
N=15: 2.10, 2.01, 1.92, 1.83, 1.75, 1.67, 1.59, 1.51, 1.43, 1.35, 1.28, 1.21,
      1.14, 1.07, 1.00
N=16: 2.10, 2.01, 1.93, 1.85, 1.77, 1.69, 1.62, 1.55, 1.48, 1.41, 1.34, 1.27,
      1.20, 1.13, 1.06, 1.00
N=17: 2.10, 2.02, 1.94, 1.86, 1.79, 1.72, 1.65, 1.58, 1.51, 1.44, 1.37, 1.30,
      1.24, 1.18, 1.12, 1.06, 1.00
```

N=18:	2.10, 2.02, 1.95, 1.88, 1.81, 1.74, 1.67, 1.60, 1.54, 1.48, 1.42, 1.36, 1.30, 1.24, 1.18, 1.12, 1.06, 1.00
N=19:	2.10, 2.03, 1.96, 1.89, 1.82, 1.76, 1.70, 1.64, 1.58, 1.52, 1.46, 1.40, 1.34, 1.28, 1.22, 1.16, 1.10, 1.05, 1.00
N=20:	2.10, 2.03, 1.96, 1.89, 1.83, 1.77, 1.71, 1.65, 1.59, 1.53, 1.47, 1.41, 1.35, 1.30, 1.25, 1.20, 1.15, 1.10, 1.05, 1.00
N=21:	2.10, 2.03, 1.97, 1.91, 1.85, 1.79, 1.73, 1.67, 1.61, 1.55, 1.50, 1.45, 1.40, 1.35, 1.30, 1.25, 1.20, 1.15, 1.10, 1.05, 1.00
N=22:	2.10, 2.04, 1.98, 1.92, 1.86, 1.80, 1.75, 1.70, 1.65, 1.60, 1.55, 1.50, 1.45, 1.40, 1.35, 1.30, 1.25, 1.20, 1.15, 1.10, 1.05, 1.00
N=23:	2.10, 2.04, 1.98, 1.92, 1.87, 1.82, 1.77, 1.72, 1.67, 1.62, 1.57, 1.52, 1.47, 1.42, 1.37, 1.32, 1.27, 1.22, 1.17, 1.12, 1.08, 1.04, 1.00
N=24:	2.10, 2.04, 1.98, 1.93, 1.88, 1.83, 1.78, 1.73, 1.68, 1.63, 1.58, 1.53, 1.48, 1.43, 1.38, 1.33, 1.28, 1.24, 1.20, 1.16, 1.12, 1.08, 1.04, 1.00
N=25:	2.10, 2.04, 1.99, 1.94, 1.89, 1.84, 1.79, 1.74, 1.69, 1.64, 1.59, 1.54, 1.49, 1.44, 1.40, 1.36, 1.32, 1.28, 1.24, 1.20, 1.16, 1.12, 1.08, 1.04, 1.00
N=26:	2.10, 2.05, 2.00, 1.95, 1.90, 1.85, 1.80, 1.75, 1.70, 1.65, 1.60, 1.56, 1.52, 1.48, 1.44, 1.40, 1.36, 1.32, 1.28, 1.24, 1.20, 1.16, 1.12, 1.08, 1.04, 1.00
N=27:	2.10, 2.05, 2.00, 1.95, 1.90, 1.85, 1.80, 1.76, 1.72, 1.68, 1.64, 1.60, 1.56, 1.52, 1.48, 1.44, 1.40, 1.36, 1.32, 1.28, 1.24, 1.20, 1.16, 1.12, 1.08, 1.04, 1.00
N=28:	2.10, 2.05, 2.00, 1.96, 1.92, 1.88, 1.84, 1.80, 1.76, 1.72, 1.68, 1.64, 1.60, 1.56, 1.52, 1.48, 1.44, 1.40, 1.36, 1.32, 1.28, 1.24, 1.20, 1.16, 1.12, 1.08, 1.04, 1.00
N=29:	2.10, 2.05, 2.01, 1.97, 1.93, 1.89, 1.85, 1.81, 1.77, 1.73, 1.69, 1.65, 1.61, 1.57, 1.53, 1.49, 1.45, 1.41, 1.37, 1.33, 1.29, 1.25, 1.21, 1.17, 1.13, 1.09, 1.06, 1.03, 1.00

N=30:	2.10, 2.06, 2.02, 1.98, 1.94, 1.90, 1.86, 1.82, 1.78, 1.74, 1.70, 1.66, 1.62, 1.58, 1.54, 1.50, 1.46, 1.42, 1.38, 1.34, 1.30, 1.26, 1.22, 1.18, 1.15, 1.12, 1.09, 1.06, 1.03, 1.00
N=31:	2.10, 2.06, 2.02, 1.98, 1.94, 1.90, 1.86, 1.82, 1.78, 1.74, 1.70, 1.66, 1.62, 1.58, 1.54, 1.50, 1.46, 1.42, 1.38, 1.34, 1.30, 1.27, 1.24, 1.21, 1.18, 1.15, 1.12, 1.09, 1.06, 1.03, 1.00
N=32:	2.10, 2.06, 2.02, 1.98, 1.94, 1.90, 1.86, 1.82, 1.78, 1.74, 1.70, 1.66, 1.62, 1.58, 1.54, 1.50, 1.46, 1.42, 1.39, 1.36, 1.33, 1.30, 1.27, 1.24, 1.21, 1.18, 1.15, 1.12, 1.09, 1.06, 1.03, 1.00
N=33:	2.10, 2.06, 2.02, 1.98, 1.94, 1.90, 1.86, 1.82, 1.78, 1.74, 1.70, 1.66, 1.62, 1.58, 1.54, 1.51, 1.48, 1.45, 1.42, 1.39, 1.36, 1.33, 1.30, 1.27, 1.24, 1.21, 1.18, 1.15, 1.12, 1.09, 1.06, 1.03, 1.00
N=34:	2.10, 2.06, 2.02, 1.98, 1.94, 1.90, 1.86, 1.82, 1.78, 1.74, 1.70, 1.66, 1.63, 1.60, 1.57, 1.54, 1.51, 1.48, 1.45, 1.42, 1.39, 1.36, 1.33, 1.30, 1.27, 1.24, 1.21, 1.18, 1.15, 1.12, 1.09, 1.06, 1.03, 1.00
N=35:	2.10, 2.06, 2.02, 1.98, 1.94, 1.90, 1.86, 1.82, 1.78, 1.75, 1.72, 1.69, 1.66, 1.63, 1.60, 1.57, 1.54, 1.51, 1.48, 1.45, 1.42, 1.39, 1.36, 1.33, 1.30, 1.27, 1.24, 1.21, 1.18, 1.15, 1.12, 1.09, 1.06, 1.03, 1.00
N=36:	2.10, 2.06, 2.02, 1.98, 1.94, 1.90, 1.87, 1.84, 1.81, 1.78, 1.75, 1.72, 1.69, 1.66, 1.63, 1.60, 1.57, 1.54, 1.51, 1.48, 1.45, 1.42, 1.39, 1.36, 1.33, 1.30, 1.27, 1.24, 1.21, 1.18, 1.15, 1.12, 1.09, 1.06, 1.03, 1.00
N=37:	2.10, 2.06, 2.02, 1.99, 1.96, 1.93, 1.90, 1.87, 1.84, 1.81, 1.78, 1.75, 1.72, 1.69, 1.66, 1.63, 1.60, 1.57, 1.54, 1.51, 1.48, 1.45, 1.42, 1.39, 1.36, 1.33, 1.30, 1.27, 1.24, 1.21, 1.18, 1.15, 1.12, 1.09, 1.06, 1.03, 1.00
N=38:	2.10, 2.07, 2.04, 2.01, 1.98, 1.95, 1.92, 1.89, 1.86, 1.83, 1.80, 1.77, 1.74, 1.71, 1.68, 1.65, 1.62, 1.59, 1.56, 1.53, 1.50, 1.47, 1.44, 1.41, 1.38, 1.35, 1.32, 1.29, 1.26, 1.23, 1.20, 1.17, 1.14, 1.11, 1.08, 1.05, 1.02, 1.00
N=39:	2.10, 2.07, 2.04, 2.01, 1.98, 1.95, 1.92, 1.89, 1.86, 1.83, 1.80, 1.77, 1.74, 1.71, 1.68, 1.65, 1.62, 1.59, 1.56, 1.53, 1.50, 1.47, 1.44, 1.41, 1.38,

1.35, 1.32, 1.29, 1.26, 1.23, 1.20, 1.17, 1.14, 1.11, 1.08, 1.06, 1.04, 1.02, 1.00
N=40: 2.10, 2.07, 2.04, 2.01, 1.98, 1.95, 1.92, 1.89, 1.86, 1.83, 1.80, 1.77, 1.74, 1.71, 1.68, 1.65, 1.62, 1.59, 1.56, 1.53, 1.50, 1.47, 1.44, 1.41, 1.38, 1.35, 1.32, 1.29, 1.26, 1.23, 1.20, 1.17, 1.14, 1.12, 1.10, 1.08, 1.06, 1.04, 1.02, 1.00
N=41: 2.10, 2.07, 2.04, 2.01, 1.98, 1.95, 1.92, 1.89, 1.86, 1.83, 1.80, 1.77, 1.74, 1.71, 1.68, 1.65, 1.62, 1.59, 1.56, 1.53, 1.50, 1.47, 1.44, 1.41, 1.38, 1.35, 1.32, 1.29, 1.26, 1.23, 1.20, 1.18, 1.16, 1.14, 1.12, 1.10, 1.08, 1.06, 1.04, 1.02, 1.00
N=42: 2.10, 2.07, 2.04, 2.01, 1.98, 1.95, 1.92, 1.89, 1.86, 1.83, 1.80, 1.77, 1.74, 1.71, 1.68, 1.65, 1.62, 1.59, 1.56, 1.53, 1.50, 1.47, 1.44, 1.41, 1.38, 1.35, 1.32, 1.29, 1.26, 1.24, 1.22, 1.20, 1.18, 1.16, 1.14, 1.12, 1.10, 1.08, 1.06, 1.04, 1.02, 1.00
N=43: 2.10, 2.07, 2.04, 2.01, 1.98, 1.95, 1.92, 1.89, 1.86, 1.83, 1.80, 1.77, 1.74, 1.71, 1.68, 1.65, 1.62, 1.59, 1.56, 1.53, 1.50, 1.47, 1.44, 1.41, 1.38, 1.35, 1.32, 1.30, 1.28, 1.26, 1.24, 1.22, 1.20, 1.18, 1.16, 1.14, 1.12, 1.10, 1.08, 1.06, 1.04, 1.02, 1.00
N=44: 2.10, 2.07, 2.04, 2.01, 1.98, 1.95, 1.92, 1.89, 1.86, 1.83, 1.80, 1.77, 1.74, 1.71, 1.68, 1.65, 1.62, 1.59, 1.56, 1.53, 1.50, 1.47, 1.44, 1.41, 1.38, 1.36, 1.34, 1.32, 1.30, 1.28, 1.26, 1.24, 1.22, 1.20, 1.18, 1.16, 1.14, 1.12, 1.10, 1.08, 1.06, 1.04, 1.02, 1.00
N=45: 2.10, 2.07, 2.04, 2.01, 1.98, 1.95, 1.92, 1.89, 1.86, 1.83, 1.80, 1.77, 1.74, 1.71, 1.68, 1.65, 1.62, 1.59, 1.56, 1.53, 1.50, 1.47, 1.44, 1.42, 1.40, 1.38, 1.36, 1.34, 1.32, 1.30, 1.28, 1.26, 1.24, 1.22, 1.20, 1.18, 1.16, 1.14, 1.12, 1.10, 1.08, 1.06, 1.04, 1.02, 1.00
N=46: 2.10, 2.07, 2.04, 2.01, 1.98, 1.95, 1.92, 1.89, 1.86, 1.83, 1.80, 1.77, 1.74, 1.71, 1.68, 1.65, 1.62, 1.59, 1.56, 1.53, 1.50, 1.48, 1.46, 1.44, 1.42, 1.40, 1.38, 1.36, 1.34, 1.32, 1.30, 1.28, 1.26, 1.24, 1.22, 1.20, 1.18, 1.16,

1.14, 1.12, 1.10, 1.08, 1.06, 1.04, 1.02, 1.00
N=47: 2.10, 2.07, 2.04, 2.01, 1.98, 1.95, 1.92, 1.89, 1.86, 1.83, 1.80, 1.77, 1.74, 1.71, 1.68, 1.65, 1.62, 1.59, 1.56, 1.54, 1.52, 1.50, 1.48, 1.46, 1.44, 1.42, 1.40, 1.38, 1.36, 1.34, 1.32, 1.30, 1.28, 1.26, 1.24, 1.22, 1.20, 1.18, 1.16, 1.14, 1.12, 1.10, 1.08, 1.06, 1.04, 1.02, 1.00
N=48: 2.10, 2.07, 2.04, 2.01, 1.98, 1.95, 1.92, 1.89, 1.86, 1.83, 1.80, 1.77, 1.74, 1.71, 1.68, 1.65, 1.62, 1.60, 1.58, 1.56, 1.54, 1.52, 1.50, 1.48, 1.46, 1.44, 1.42, 1.40, 1.38, 1.36, 1.34, 1.32, 1.30, 1.28, 1.26, 1.24, 1.22, 1.20, 1.18, 1.16, 1.14, 1.12, 1.10, 1.08, 1.06, 1.04, 1.02, 1.00
N=49: 2.10, 2.07, 2.04, 2.01, 1.98, 1.95, 1.92, 1.89, 1.86, 1.83, 1.80, 1.77, 1.74, 1.71, 1.68, 1.66, 1.64, 1.62, 1.60, 1.58, 1.56, 1.54, 1.52, 1.50, 1.48, 1.46, 1.44, 1.42, 1.40, 1.38, 1.36, 1.34, 1.32, 1.30, 1.28, 1.26, 1.24, 1.22, 1.20, 1.18, 1.16, 1.14, 1.12, 1.10, 1.08, 1.06, 1.04, 1.02, 1.00
N=50: 2.10, 2.07, 2.04, 2.01, 1.98, 1.95, 1.92, 1.89, 1.86, 1.83, 1.80, 1.77, 1.74, 1.72, 1.70, 1.68, 1.66, 1.64, 1.62, 1.60, 1.58, 1.56, 1.54, 1.52, 1.50, 1.48, 1.46, 1.44, 1.42, 1.40, 1.38, 1.36, 1.34, 1.32, 1.30, 1.28, 1.26, 1.24, 1.22, 1.20, 1.18, 1.16, 1.14, 1.12, 1.10, 1.08, 1.06, 1.04, 1.02, 1.00

Unconstrained bandgaps (full concentration)

N= 1: 1.07
N= 2: 1.65, 0.75
N= 3: 2.03, 1.21, 0.59
N= 4: 2.33, 1.55, 0.99, 0.49
N= 5: 2.55, 1.81, 1.29, 0.85, 0.43
N= 6: 2.77, 2.05, 1.55, 1.13, 0.75, 0.37
N= 7: 2.95, 2.23, 1.75, 1.35, 1.01, 0.69, 0.35
N= 8: 3.09, 2.39, 1.91, 1.53, 1.21, 0.91, 0.61, 0.31
N= 9: 3.23, 2.53, 2.07, 1.69, 1.37, 1.09, 0.83, 0.57, 0.29

N=10:	3.35, 2.67, 2.21, 1.85, 1.55, 1.27, 1.01, 0.77, 0.53, 0.27
N=11:	3.49, 2.81, 2.35, 1.99, 1.69, 1.43, 1.19, 0.95, 0.73, 0.51, 0.25
N=12:	3.59, 2.91, 2.47, 2.13, 1.83, 1.57, 1.33, 1.11, 0.89, 0.69, 0.47, 0.23
N=13:	3.67, 3.01, 2.57, 2.23, 1.95, 1.69, 1.45, 1.23, 1.03, 0.83, 0.63, 0.43, 0.21
N=14:	3.77, 3.11, 2.67, 2.33, 2.05, 1.79, 1.57, 1.37, 1.17, 0.99, 0.81, 0.63, 0.43, 0.21
N=15:	3.87, 3.21, 2.77, 2.43, 2.15, 1.91, 1.69, 1.49, 1.29, 1.11, 0.93, 0.75, 0.57, 0.39, 0.19
N=16:	3.95, 3.29, 2.85, 2.51, 2.23, 1.99, 1.77, 1.57, 1.39, 1.21, 1.05, 0.89, 0.73, 0.57, 0.39, 0.19
N=17:	4.07, 3.41, 2.97, 2.63, 2.35, 2.11, 1.89, 1.69, 1.51, 1.33, 1.17, 1.01, 0.85, 0.69, 0.53, 0.37, 0.17
N=18:	4.11, 3.47, 3.05, 2.71, 2.43, 2.19, 1.97, 1.77, 1.59, 1.43, 1.27, 1.11, 0.95, 0.81, 0.67, 0.51, 0.35, 0.17
N=19:	4.15, 3.51, 3.09, 2.77, 2.49, 2.25, 2.05, 1.85, 1.67, 1.51, 1.35, 1.19, 1.05, 0.91, 0.77, 0.63, 0.49, 0.33, 0.15
N=20:	4.23, 3.59, 3.17, 2.85, 2.57, 2.33, 2.13, 1.95, 1.77, 1.61, 1.45, 1.31, 1.17, 1.03, 0.89, 0.75, 0.61, 0.47, 0.33, 0.15
N=21:	4.29, 3.65, 3.23, 2.91, 2.65, 2.41, 2.21, 2.03, 1.85, 1.69, 1.53, 1.39, 1.25, 1.11, 0.97, 0.85, 0.73, 0.59, 0.45, 0.31, 0.13
N=22:	4.35, 3.71, 3.29, 2.97, 2.71, 2.47, 2.27, 2.09, 1.91, 1.75, 1.61, 1.47, 1.33, 1.19, 1.07, 0.95, 0.83, 0.71, 0.59, 0.45, 0.31, 0.13
N=23:	4.39, 3.75, 3.33, 3.01, 2.75, 2.53, 2.33, 2.15, 1.99, 1.83, 1.69, 1.55, 1.41, 1.27, 1.15, 1.03, 0.91, 0.79, 0.67, 0.55, 0.43, 0.29, 0.13
N=24:	4.49, 3.85, 3.43, 3.11, 2.85, 2.63, 2.43, 2.25, 2.09, 1.93, 1.79, 1.65, 1.51, 1.39, 1.27, 1.15, 1.03, 0.91, 0.79, 0.67, 0.55, 0.43, 0.29, 0.13
N=25:	4.57, 3.93, 3.51, 3.19, 2.93, 2.71, 2.51, 2.33, 2.17, 2.01, 1.87, 1.73, 1.59, 1.47, 1.35, 1.23, 1.11, 0.99, 0.87, 0.75, 0.63, 0.51, 0.39, 0.27, 0.11

N=26: 4.59, 3.95, 3.53, 3.21, 2.95, 2.73, 2.53, 2.35, 2.19, 2.03, 1.89, 1.75,
 1.63, 1.51, 1.39, 1.27, 1.15, 1.03, 0.93, 0.83, 0.73, 0.63, 0.51, 0.39, 0.27,
 0.11

N=27: 4.65, 4.01, 3.59, 3.27, 3.01, 2.79, 2.59, 2.41, 2.25, 2.09, 1.95, 1.81,
 1.69, 1.57, 1.45, 1.33, 1.21, 1.11, 1.01, 0.91, 0.81, 0.71, 0.61, 0.51, 0.39,
 0.27, 0.11

N=28: 4.69, 4.07, 3.65, 3.33, 3.07, 2.85, 2.65, 2.47, 2.31, 2.15, 2.01, 1.87,
 1.75, 1.63, 1.51, 1.39, 1.29, 1.19, 1.09, 0.99, 0.89, 0.79, 0.69, 0.59, 0.49,
 0.37, 0.25, 0.11

N=29: 4.75, 4.13, 3.71, 3.39, 3.13, 2.91, 2.71, 2.53, 2.37, 2.23, 2.09, 1.95,
 1.83, 1.71, 1.59, 1.47, 1.37, 1.27, 1.17, 1.07, 0.97, 0.87, 0.77, 0.67, 0.57,
 0.47, 0.37, 0.25, 0.11

N=30: 4.81, 4.19, 3.77, 3.45, 3.19, 2.97, 2.77, 2.59, 2.43, 2.29, 2.15, 2.01,
 1.89, 1.77, 1.65, 1.55, 1.45, 1.35, 1.25, 1.15, 1.05, 0.95, 0.85, 0.75, 0.65,
 0.55, 0.45, 0.35, 0.23, 0.09

N=31: 4.87, 4.25, 3.85, 3.53, 3.27, 3.05, 2.85, 2.67, 2.51, 2.37, 2.23, 2.11,
 1.99, 1.87, 1.75, 1.65, 1.55, 1.45, 1.35, 1.25, 1.15, 1.05, 0.95, 0.85, 0.75,
 0.65, 0.55, 0.45, 0.35, 0.23, 0.09

N=32: 4.89, 4.27, 3.87, 3.55, 3.29, 3.07, 2.87, 2.69, 2.53, 2.39, 2.25, 2.13,
 2.01, 1.89, 1.77, 1.67, 1.57, 1.47, 1.37, 1.27, 1.17, 1.07, 0.97, 0.89, 0.81,
 0.73, 0.63, 0.53, 0.43, 0.33, 0.23, 0.09

N=33: 4.93, 4.31, 3.91, 3.59, 3.33, 3.11, 2.91, 2.73, 2.57, 2.43, 2.29, 2.17,
 2.05, 1.93, 1.81, 1.71, 1.61, 1.51, 1.41, 1.31, 1.21, 1.11, 1.03, 0.95, 0.87,
 0.79, 0.71, 0.63, 0.53, 0.43, 0.33, 0.23, 0.09

N=34: 4.97, 4.35, 3.95, 3.63, 3.37, 3.15, 2.95, 2.77, 2.61, 2.47, 2.33, 2.21,
 2.09, 1.97, 1.85, 1.75, 1.65, 1.55, 1.45, 1.35, 1.25, 1.17, 1.09, 1.01, 0.93,
 0.85, 0.77, 0.69, 0.61, 0.53, 0.43, 0.33, 0.23, 0.09

N=35: 5.01, 4.39, 3.99, 3.67, 3.41, 3.19, 2.99, 2.81, 2.65, 2.51, 2.37, 2.25,
 2.13, 2.01, 1.91, 1.81, 1.71, 1.61, 1.51, 1.41, 1.31, 1.23, 1.15, 1.07, 0.99,

0.91, 0.83, 0.75, 0.67, 0.59, 0.51, 0.41, 0.31, 0.21, 0.07
N=36: 5.03, 4.41, 4.01, 3.71, 3.45, 3.23, 3.03, 2.85, 2.69, 2.55, 2.41, 2.29, 2.17, 2.05, 1.95, 1.85, 1.75, 1.65, 1.55, 1.45, 1.37, 1.29, 1.21, 1.13, 1.05, 0.97, 0.89, 0.81, 0.73, 0.65, 0.57, 0.49, 0.41, 0.31, 0.21, 0.07
N=37: 5.11, 4.49, 4.09, 3.79, 3.53, 3.31, 3.11, 2.93, 2.77, 2.63, 2.49, 2.37, 2.25, 2.13, 2.03, 1.93, 1.83, 1.73, 1.63, 1.53, 1.45, 1.37, 1.29, 1.21, 1.13, 1.05, 0.97, 0.89, 0.81, 0.73, 0.65, 0.57, 0.49, 0.41, 0.31, 0.21, 0.07
N=38: 5.15, 4.53, 4.13, 3.83, 3.57, 3.35, 3.15, 2.97, 2.81, 2.67, 2.53, 2.41, 2.29, 2.17, 2.07, 1.97, 1.87, 1.77, 1.67, 1.59, 1.51, 1.43, 1.35, 1.27, 1.19, 1.11, 1.03, 0.95, 0.87, 0.79, 0.71, 0.63, 0.55, 0.47, 0.39, 0.31, 0.21, 0.07
N=39: 5.19, 4.57, 4.17, 3.87, 3.61, 3.39, 3.21, 3.03, 2.87, 2.73, 2.59, 2.47, 2.35, 2.23, 2.13, 2.03, 1.93, 1.83, 1.73, 1.65, 1.57, 1.49, 1.41, 1.33, 1.25, 1.17, 1.09, 1.01, 0.93, 0.85, 0.77, 0.69, 0.61, 0.53, 0.45, 0.37, 0.29, 0.19, 0.07
N=40: 5.25, 4.63, 4.23, 3.93, 3.67, 3.45, 3.27, 3.11, 2.95, 2.81, 2.67, 2.55, 2.43, 2.31, 2.21, 2.11, 2.01, 1.91, 1.81, 1.73, 1.65, 1.57, 1.49, 1.41, 1.33, 1.25, 1.17, 1.09, 1.01, 0.93, 0.85, 0.77, 0.69, 0.61, 0.53, 0.45, 0.37, 0.29, 0.19, 0.07
N=41: 5.29, 4.67, 4.27, 3.97, 3.71, 3.49, 3.31, 3.15, 2.99, 2.85, 2.71, 2.59, 2.47, 2.35, 2.25, 2.15, 2.05, 1.95, 1.87, 1.79, 1.71, 1.63, 1.55, 1.47, 1.39, 1.31, 1.23, 1.15, 1.07, 0.99, 0.91, 0.83, 0.75, 0.67, 0.59, 0.51, 0.43, 0.35, 0.27, 0.17, 0.05
N=42: 5.33, 4.71, 4.31, 4.01, 3.75, 3.53, 3.35, 3.19, 3.03, 2.89, 2.75, 2.63, 2.51, 2.39, 2.29, 2.19, 2.09, 1.99, 1.91, 1.83, 1.75, 1.67, 1.59, 1.51, 1.43, 1.35, 1.27, 1.19, 1.11, 1.03, 0.95, 0.87, 0.81, 0.75, 0.67, 0.59, 0.51, 0.43, 0.35, 0.27, 0.17, 0.05
N=43: 5.33, 4.71, 4.31, 4.01, 3.75, 3.53, 3.35, 3.19, 3.03, 2.89, 2.75, 2.63, 2.51, 2.39, 2.29, 2.19, 2.09, 1.99, 1.91, 1.83, 1.75, 1.67, 1.59, 1.51, 1.43, 1.35, 1.27, 1.19, 1.11, 1.03, 0.97, 0.91, 0.85, 0.79, 0.73, 0.67, 0.59, 0.51,

0.43, 0.35, 0.27, 0.17, 0.05
N=44: 5.33, 4.71, 4.31, 4.01, 3.77, 3.55, 3.37, 3.21, 3.05, 2.91, 2.77, 2.65, 2.53, 2.43, 2.33, 2.23, 2.13, 2.03, 1.95, 1.87, 1.79, 1.71, 1.63, 1.55, 1.47, 1.39, 1.31, 1.23, 1.15, 1.07, 1.01, 0.95, 0.89, 0.83, 0.77, 0.71, 0.65, 0.59, 0.51, 0.43, 0.35, 0.27, 0.17, 0.05
N=45: 5.37, 4.75, 4.35, 4.05, 3.81, 3.59, 3.41, 3.25, 3.09, 2.95, 2.81, 2.69, 2.57, 2.47, 2.37, 2.27, 2.17, 2.07, 1.99, 1.91, 1.83, 1.75, 1.67, 1.59, 1.51, 1.43, 1.35, 1.27, 1.19, 1.13, 1.07, 1.01, 0.95, 0.89, 0.83, 0.77, 0.71, 0.65, 0.59, 0.51, 0.43, 0.35, 0.27, 0.17, 0.05
N=46: 5.39, 4.77, 4.37, 4.07, 3.83, 3.61, 3.43, 3.27, 3.11, 2.97, 2.83, 2.71, 2.59, 2.49, 2.39, 2.29, 2.19, 2.09, 2.01, 1.93, 1.85, 1.77, 1.69, 1.61, 1.53, 1.45, 1.37, 1.29, 1.23, 1.17, 1.11, 1.05, 0.99, 0.93, 0.87, 0.81, 0.75, 0.69, 0.63, 0.57, 0.51, 0.43, 0.35, 0.27, 0.17, 0.05
N=47: 5.43, 4.81, 4.41, 4.11, 3.87, 3.65, 3.47, 3.31, 3.15, 3.01, 2.87, 2.75, 2.63, 2.53, 2.43, 2.33, 2.23, 2.13, 2.05, 1.97, 1.89, 1.81, 1.73, 1.65, 1.57, 1.49, 1.41, 1.33, 1.27, 1.21, 1.15, 1.09, 1.03, 0.97, 0.91, 0.85, 0.79, 0.73, 0.67, 0.61, 0.55, 0.49, 0.41, 0.33, 0.25, 0.17, 0.05
N=48: 5.45, 4.83, 4.43, 4.13, 3.89, 3.67, 3.49, 3.33, 3.17, 3.03, 2.89, 2.77, 2.65, 2.55, 2.45, 2.35, 2.25, 2.15, 2.07, 1.99, 1.91, 1.83, 1.75, 1.67, 1.59, 1.51, 1.43, 1.37, 1.31, 1.25, 1.19, 1.13, 1.07, 1.01, 0.95, 0.89, 0.83, 0.77, 0.71, 0.65, 0.59, 0.53, 0.47, 0.41, 0.33, 0.25, 0.17, 0.05
N=49: 5.49, 4.87, 4.47, 4.17, 3.93, 3.71, 3.53, 3.37, 3.21, 3.07, 2.95, 2.83, 2.71, 2.61, 2.51, 2.41, 2.31, 2.21, 2.13, 2.05, 1.97, 1.89, 1.81, 1.73, 1.65, 1.57, 1.49, 1.43, 1.37, 1.31, 1.25, 1.19, 1.13, 1.07, 1.01, 0.95, 0.89, 0.83, 0.77, 0.71, 0.65, 0.59, 0.53, 0.47, 0.41, 0.33, 0.25, 0.17, 0.05
N=50: 5.51, 4.89, 4.49, 4.19, 3.95, 3.73, 3.55, 3.39, 3.23, 3.09, 2.97, 2.85, 2.73, 2.63, 2.53, 2.43, 2.33, 2.23, 2.15, 2.07, 1.99, 1.91, 1.83, 1.75, 1.67, 1.59, 1.53, 1.47, 1.41, 1.35, 1.29, 1.23, 1.17, 1.11, 1.05, 0.99, 0.93, 0.87, 0.81, 0.75, 0.69, 0.63, 0.57, 0.51, 0.45, 0.39, 0.33, 0.25, 0.17, 0.05

Conservative TMD window (1 sun)

```
N= 1: 1.28
N= 2: 1.85, 1.00
N= 3: 2.10, 1.49, 1.00
N= 4: 2.10, 1.68, 1.32, 1.00
N= 5: 2.10, 1.78, 1.50, 1.24, 1.00
N= 6: 2.10, 1.84, 1.61, 1.39, 1.19, 1.00
N= 7: 2.10, 1.88, 1.68, 1.50, 1.33, 1.16, 1.00
N= 8: 2.10, 1.91, 1.74, 1.58, 1.43, 1.28, 1.14, 1.00
N= 9: 2.10, 1.94, 1.79, 1.64, 1.50, 1.37, 1.24, 1.12, 1.00
N=10: 2.10, 1.96, 1.82, 1.69, 1.57, 1.45, 1.33, 1.22, 1.11, 1.00
N=11: 2.10, 1.97, 1.85, 1.73, 1.62, 1.51, 1.40, 1.30, 1.20, 1.10, 1.00
N=12: 2.10, 1.98, 1.87, 1.76, 1.66, 1.56, 1.46, 1.36, 1.27, 1.18, 1.09, 1.00
N=13: 2.10, 1.99, 1.89, 1.79, 1.69, 1.60, 1.51, 1.42, 1.33, 1.24, 1.16, 1.08,
      1.00
N=14: 2.10, 2.00, 1.90, 1.81, 1.72, 1.63, 1.55, 1.47, 1.39, 1.31, 1.23, 1.15,
      1.07, 1.00
N=15: 2.10, 2.01, 1.92, 1.83, 1.75, 1.67, 1.59, 1.51, 1.43, 1.35, 1.28, 1.21,
      1.14, 1.07, 1.00
N=16: 2.10, 2.01, 1.93, 1.85, 1.77, 1.69, 1.62, 1.55, 1.48, 1.41, 1.34, 1.27,
      1.20, 1.13, 1.06, 1.00
N=17: 2.10, 2.02, 1.94, 1.86, 1.79, 1.72, 1.65, 1.58, 1.51, 1.44, 1.37, 1.30,
      1.24, 1.18, 1.12, 1.06, 1.00
N=18: 2.10, 2.02, 1.95, 1.88, 1.81, 1.74, 1.67, 1.60, 1.54, 1.48, 1.42, 1.36,
      1.30, 1.24, 1.18, 1.12, 1.06, 1.00
```

N=19:	2.10, 2.03, 1.96, 1.89, 1.82, 1.76, 1.70, 1.64, 1.58, 1.52, 1.46, 1.40, 1.34, 1.28, 1.22, 1.16, 1.10, 1.05, 1.00
N=20:	2.10, 2.03, 1.96, 1.89, 1.83, 1.77, 1.71, 1.65, 1.59, 1.53, 1.47, 1.41, 1.35, 1.30, 1.25, 1.20, 1.15, 1.10, 1.05, 1.00
N=21:	2.10, 2.03, 1.97, 1.91, 1.85, 1.79, 1.73, 1.67, 1.61, 1.55, 1.50, 1.45, 1.40, 1.35, 1.30, 1.25, 1.20, 1.15, 1.10, 1.05, 1.00
N=22:	2.10, 2.04, 1.98, 1.92, 1.86, 1.80, 1.75, 1.70, 1.65, 1.60, 1.55, 1.50, 1.45, 1.40, 1.35, 1.30, 1.25, 1.20, 1.15, 1.10, 1.05, 1.00
N=23:	2.10, 2.04, 1.98, 1.92, 1.87, 1.82, 1.77, 1.72, 1.67, 1.62, 1.57, 1.52, 1.47, 1.42, 1.37, 1.32, 1.27, 1.22, 1.17, 1.12, 1.08, 1.04, 1.00
N=24:	2.10, 2.04, 1.98, 1.93, 1.88, 1.83, 1.78, 1.73, 1.68, 1.63, 1.58, 1.53, 1.48, 1.43, 1.38, 1.33, 1.28, 1.24, 1.20, 1.16, 1.12, 1.08, 1.04, 1.00
N=25:	2.10, 2.05, 2.00, 1.95, 1.90, 1.85, 1.80, 1.75, 1.70, 1.65, 1.60, 1.55, 1.50, 1.45, 1.40, 1.36, 1.32, 1.28, 1.24, 1.20, 1.16, 1.12, 1.08, 1.04, 1.00
N=26:	2.10, 2.05, 2.00, 1.95, 1.90, 1.85, 1.80, 1.75, 1.70, 1.65, 1.60, 1.56, 1.52, 1.48, 1.44, 1.40, 1.36, 1.32, 1.28, 1.24, 1.20, 1.16, 1.12, 1.08, 1.04, 1.00
N=27:	2.10, 2.05, 2.00, 1.95, 1.90, 1.85, 1.80, 1.76, 1.72, 1.68, 1.64, 1.60, 1.56, 1.52, 1.48, 1.44, 1.40, 1.36, 1.32, 1.28, 1.24, 1.20, 1.16, 1.12, 1.08, 1.04, 1.00
N=28:	2.10, 2.05, 2.00, 1.96, 1.92, 1.88, 1.84, 1.80, 1.76, 1.72, 1.68, 1.64, 1.60, 1.56, 1.52, 1.48, 1.44, 1.40, 1.36, 1.32, 1.28, 1.24, 1.20, 1.16, 1.12, 1.08, 1.04, 1.00
N=29:	2.10, 2.05, 2.01, 1.97, 1.93, 1.89, 1.85, 1.81, 1.77, 1.73, 1.69, 1.65, 1.61, 1.57, 1.53, 1.49, 1.45, 1.41, 1.37, 1.33, 1.29, 1.25, 1.21, 1.17, 1.13, 1.09, 1.06, 1.03, 1.00
N=30:	2.10, 2.06, 2.02, 1.98, 1.94, 1.90, 1.86, 1.82, 1.78, 1.74, 1.70, 1.66, 1.62, 1.58, 1.54, 1.50, 1.46, 1.42, 1.38, 1.34, 1.30, 1.26, 1.22, 1.18, 1.15, 1.12, 1.09, 1.06, 1.03, 1.00

N=31:	2.10, 2.06, 2.02, 1.98, 1.94, 1.90, 1.86, 1.82, 1.78, 1.74, 1.70, 1.66, 1.62, 1.58, 1.54, 1.50, 1.46, 1.42, 1.38, 1.34, 1.30, 1.27, 1.24, 1.21, 1.18, 1.15, 1.12, 1.09, 1.06, 1.03, 1.00
N=32:	2.10, 2.06, 2.02, 1.98, 1.94, 1.90, 1.86, 1.82, 1.78, 1.74, 1.70, 1.66, 1.62, 1.58, 1.54, 1.50, 1.46, 1.42, 1.39, 1.36, 1.33, 1.30, 1.27, 1.24, 1.21, 1.18, 1.15, 1.12, 1.09, 1.06, 1.03, 1.00
N=33:	2.10, 2.06, 2.02, 1.98, 1.94, 1.90, 1.86, 1.82, 1.78, 1.74, 1.70, 1.66, 1.62, 1.58, 1.54, 1.51, 1.48, 1.45, 1.42, 1.39, 1.36, 1.33, 1.30, 1.27, 1.24, 1.21, 1.18, 1.15, 1.12, 1.09, 1.06, 1.03, 1.00
N=34:	2.10, 2.06, 2.02, 1.98, 1.94, 1.90, 1.86, 1.82, 1.78, 1.74, 1.70, 1.66, 1.63, 1.60, 1.57, 1.54, 1.51, 1.48, 1.45, 1.42, 1.39, 1.36, 1.33, 1.30, 1.27, 1.24, 1.21, 1.18, 1.15, 1.12, 1.09, 1.06, 1.03, 1.00
N=35:	2.10, 2.06, 2.02, 1.98, 1.94, 1.90, 1.86, 1.82, 1.78, 1.75, 1.72, 1.69, 1.63, 1.60, 1.57, 1.54, 1.51, 1.48, 1.45, 1.42, 1.39, 1.36, 1.33, 1.30, 1.27, 1.24, 1.21, 1.18, 1.15, 1.12, 1.09, 1.06, 1.03, 1.00
N=36:	2.10, 2.06, 2.02, 1.98, 1.94, 1.90, 1.87, 1.84, 1.81, 1.78, 1.75, 1.72, 1.69, 1.66, 1.63, 1.60, 1.57, 1.54, 1.51, 1.48, 1.45, 1.42, 1.39, 1.36, 1.33, 1.30, 1.27, 1.24, 1.21, 1.18, 1.15, 1.12, 1.09, 1.06, 1.03, 1.00
N=37:	2.10, 2.06, 2.02, 1.99, 1.96, 1.93, 1.90, 1.87, 1.84, 1.81, 1.78, 1.75, 1.72, 1.69, 1.66, 1.63, 1.60, 1.57, 1.54, 1.51, 1.48, 1.45, 1.42, 1.39, 1.36, 1.33, 1.30, 1.27, 1.24, 1.21, 1.18, 1.15, 1.12, 1.09, 1.06, 1.03, 1.00
N=38:	2.10, 2.07, 2.04, 2.01, 1.98, 1.95, 1.92, 1.89, 1.86, 1.83, 1.80, 1.77, 1.74, 1.71, 1.68, 1.65, 1.62, 1.59, 1.56, 1.53, 1.50, 1.47, 1.44, 1.41, 1.38, 1.35, 1.32, 1.29, 1.26, 1.23, 1.20, 1.17, 1.14, 1.11, 1.08, 1.05, 1.02, 1.00
N=39:	2.10, 2.07, 2.04, 2.01, 1.98, 1.95, 1.92, 1.89, 1.86, 1.83, 1.80, 1.77, 1.74, 1.71, 1.68, 1.65, 1.62, 1.59, 1.56, 1.53, 1.50, 1.47, 1.44, 1.41, 1.38, 1.35, 1.32, 1.29, 1.26, 1.23, 1.20, 1.17, 1.14, 1.11, 1.08, 1.06, 1.04, 1.02, 1.00

N=40:	2.10, 2.07, 2.04, 2.01, 1.98, 1.95, 1.92, 1.89, 1.86, 1.83, 1.80, 1.77, 1.74, 1.71, 1.68, 1.65, 1.62, 1.59, 1.56, 1.53, 1.50, 1.47, 1.44, 1.41, 1.38, 1.35, 1.32, 1.29, 1.26, 1.23, 1.20, 1.17, 1.14, 1.12, 1.10, 1.08, 1.06, 1.04, 1.02, 1.00
N=41:	2.10, 2.07, 2.04, 2.01, 1.98, 1.95, 1.92, 1.89, 1.86, 1.83, 1.80, 1.77, 1.74, 1.71, 1.68, 1.65, 1.62, 1.59, 1.56, 1.53, 1.50, 1.47, 1.44, 1.41, 1.38, 1.35, 1.32, 1.29, 1.26, 1.23, 1.20, 1.18, 1.16, 1.14, 1.12, 1.10, 1.08, 1.06, 1.04, 1.02, 1.00
N=42:	2.10, 2.07, 2.04, 2.01, 1.98, 1.95, 1.92, 1.89, 1.86, 1.83, 1.80, 1.77, 1.74, 1.71, 1.68, 1.65, 1.62, 1.59, 1.56, 1.53, 1.50, 1.47, 1.44, 1.41, 1.38, 1.35, 1.32, 1.29, 1.26, 1.24, 1.22, 1.20, 1.18, 1.16, 1.14, 1.12, 1.10, 1.08, 1.06, 1.04, 1.02, 1.00
N=43:	2.10, 2.07, 2.04, 2.01, 1.98, 1.95, 1.92, 1.89, 1.86, 1.83, 1.80, 1.77, 1.74, 1.71, 1.68, 1.65, 1.62, 1.59, 1.56, 1.53, 1.50, 1.47, 1.44, 1.41, 1.38, 1.35, 1.32, 1.30, 1.28, 1.26, 1.24, 1.22, 1.20, 1.18, 1.16, 1.14, 1.12, 1.10, 1.08, 1.06, 1.04, 1.02, 1.00
N=44:	2.10, 2.07, 2.04, 2.01, 1.98, 1.95, 1.92, 1.89, 1.86, 1.83, 1.80, 1.77, 1.74, 1.71, 1.68, 1.65, 1.62, 1.59, 1.56, 1.53, 1.50, 1.47, 1.44, 1.41, 1.38, 1.36, 1.34, 1.32, 1.30, 1.28, 1.26, 1.24, 1.22, 1.20, 1.18, 1.16, 1.14, 1.12, 1.10, 1.08, 1.06, 1.04, 1.02, 1.00
N=45:	2.10, 2.07, 2.04, 2.01, 1.98, 1.95, 1.92, 1.89, 1.86, 1.83, 1.80, 1.77, 1.74, 1.71, 1.68, 1.65, 1.62, 1.59, 1.56, 1.53, 1.50, 1.47, 1.44, 1.42, 1.40, 1.38, 1.36, 1.34, 1.32, 1.30, 1.28, 1.26, 1.24, 1.22, 1.20, 1.18, 1.16, 1.14, 1.12, 1.10, 1.08, 1.06, 1.04, 1.02, 1.00
N=46:	2.10, 2.07, 2.04, 2.01, 1.98, 1.95, 1.92, 1.89, 1.86, 1.83, 1.80, 1.77, 1.74, 1.71, 1.68, 1.65, 1.62, 1.59, 1.56, 1.53, 1.50, 1.48, 1.46, 1.44, 1.42, 1.40, 1.38, 1.36, 1.34, 1.32, 1.30, 1.28, 1.26, 1.24, 1.22, 1.20, 1.18, 1.16, 1.14, 1.12, 1.10, 1.08, 1.06, 1.04, 1.02, 1.00

N=47: 2.10, 2.07, 2.04, 2.01, 1.98, 1.95, 1.92, 1.89, 1.86, 1.83, 1.80, 1.77, 1.74, 1.71, 1.68, 1.65, 1.62, 1.59, 1.56, 1.54, 1.52, 1.50, 1.48, 1.46, 1.44, 1.42, 1.40, 1.38, 1.36, 1.34, 1.32, 1.30, 1.28, 1.26, 1.24, 1.22, 1.20, 1.18, 1.16, 1.14, 1.12, 1.10, 1.08, 1.06, 1.04, 1.02, 1.00
N=48: 2.10, 2.07, 2.04, 2.01, 1.98, 1.95, 1.92, 1.89, 1.86, 1.83, 1.80, 1.77, 1.74, 1.71, 1.68, 1.65, 1.62, 1.60, 1.58, 1.56, 1.54, 1.52, 1.50, 1.48, 1.46, 1.44, 1.42, 1.40, 1.38, 1.36, 1.34, 1.32, 1.30, 1.28, 1.26, 1.24, 1.22, 1.20, 1.18, 1.16, 1.14, 1.12, 1.10, 1.08, 1.06, 1.04, 1.02, 1.00
N=49: 2.10, 2.07, 2.04, 2.01, 1.98, 1.95, 1.92, 1.89, 1.86, 1.83, 1.80, 1.77, 1.74, 1.71, 1.68, 1.66, 1.64, 1.62, 1.60, 1.58, 1.56, 1.54, 1.52, 1.50, 1.48, 1.46, 1.44, 1.42, 1.40, 1.38, 1.36, 1.34, 1.32, 1.30, 1.28, 1.26, 1.24, 1.22, 1.20, 1.18, 1.16, 1.14, 1.12, 1.10, 1.08, 1.06, 1.04, 1.02, 1.00
N=50: 2.10, 2.07, 2.04, 2.01, 1.98, 1.95, 1.92, 1.89, 1.86, 1.83, 1.80, 1.77, 1.74, 1.72, 1.70, 1.68, 1.66, 1.64, 1.62, 1.60, 1.58, 1.56, 1.54, 1.52, 1.50, 1.48, 1.46, 1.44, 1.42, 1.40, 1.38, 1.36, 1.34, 1.32, 1.30, 1.28, 1.26, 1.24, 1.22, 1.20, 1.18, 1.16, 1.14, 1.12, 1.10, 1.08, 1.06, 1.04, 1.02, 1.00

Unconstrained bandgaps (1 sun)

N= 1: 1.27
N= 2: 1.83, 0.97
N= 3: 2.19, 1.39, 0.81
N= 4: 2.49, 1.73, 1.19, 0.73
N= 5: 2.71, 1.97, 1.47, 1.05, 0.65
N= 6: 2.91, 2.19, 1.71, 1.31, 0.95, 0.61
N= 7: 3.07, 2.37, 1.89, 1.51, 1.17, 0.87, 0.57
N= 8: 3.23, 2.53, 2.07, 1.71, 1.39, 1.11, 0.83, 0.55
N= 9: 3.35, 2.67, 2.21, 1.85, 1.55, 1.27, 1.01, 0.77, 0.53
N=10: 3.49, 2.81, 2.35, 1.99, 1.69, 1.43, 1.19, 0.97, 0.75, 0.51

N=11:	3.61, 2.93, 2.49, 2.15, 1.85, 1.59, 1.35, 1.13, 0.91, 0.71, 0.49
N=12:	3.69, 3.03, 2.59, 2.25, 1.97, 1.71, 1.49, 1.27, 1.07, 0.87, 0.67, 0.47
N=13:	3.79, 3.13, 2.69, 2.35, 2.07, 1.83, 1.61, 1.41, 1.21, 1.03, 0.85, 0.67, 0.47
N=14:	3.91, 3.25, 2.81, 2.47, 2.19, 1.95, 1.73, 1.53, 1.35, 1.17, 0.99, 0.81, 0.63, 0.45
N=15:	4.01, 3.35, 2.91, 2.57, 2.29, 2.05, 1.83, 1.63, 1.45, 1.27, 1.11, 0.95, 0.79, 0.63, 0.45
N=16:	4.07, 3.43, 3.01, 2.67, 2.39, 2.15, 1.93, 1.73, 1.55, 1.39, 1.23, 1.07, 0.91, 0.75, 0.59, 0.43
N=17:	4.13, 3.49, 3.07, 2.75, 2.47, 2.23, 2.01, 1.81, 1.63, 1.47, 1.31, 1.15, 1.01, 0.87, 0.73, 0.59, 0.43
N=18:	4.19, 3.55, 3.13, 2.81, 2.53, 2.29, 2.09, 1.91, 1.73, 1.57, 1.41, 1.27, 1.13, 0.99, 0.85, 0.71, 0.57, 0.41
N=19:	4.29, 3.65, 3.23, 2.91, 2.65, 2.41, 2.21, 2.03, 1.85, 1.69, 1.53, 1.39, 1.25, 1.11, 0.97, 0.83, 0.69, 0.55, 0.41
N=20:	4.35, 3.71, 3.29, 2.97, 2.71, 2.47, 2.27, 2.09, 1.91, 1.75, 1.59, 1.45, 1.31, 1.17, 1.05, 0.93, 0.81, 0.69, 0.55, 0.41
N=21:	4.39, 3.75, 3.33, 3.01, 2.75, 2.53, 2.33, 2.15, 1.99, 1.83, 1.69, 1.55, 1.41, 1.27, 1.15, 1.03, 0.91, 0.79, 0.67, 0.55, 0.41
N=22:	4.47, 3.83, 3.41, 3.09, 2.83, 2.61, 2.41, 2.23, 2.07, 1.91, 1.77, 1.63, 1.49, 1.37, 1.25, 1.13, 1.01, 0.89, 0.77, 0.65, 0.53, 0.39
N=23:	4.57, 3.93, 3.51, 3.19, 2.93, 2.71, 2.51, 2.33, 2.17, 2.01, 1.87, 1.73, 1.59, 1.47, 1.35, 1.23, 1.11, 0.99, 0.87, 0.75, 0.63, 0.51, 0.39
N=24:	4.61, 3.97, 3.55, 3.23, 2.97, 2.75, 2.55, 2.37, 2.21, 2.05, 1.91, 1.77, 1.65, 1.53, 1.41, 1.29, 1.17, 1.05, 0.95, 0.85, 0.75, 0.63, 0.51, 0.39
N=25:	4.67, 4.03, 3.61, 3.29, 3.03, 2.81, 2.61, 2.43, 2.27, 2.11, 1.97, 1.83, 1.71, 1.59, 1.47, 1.35, 1.23, 1.13, 1.03, 0.93, 0.83, 0.73, 0.63, 0.51, 0.39

N=26:	4.69, 4.07, 3.65, 3.33, 3.07, 2.85, 2.65, 2.47, 2.31, 2.15, 2.01, 1.87, 1.75, 1.63, 1.51, 1.39, 1.29, 1.19, 1.09, 0.99, 0.89, 0.79, 0.69, 0.59, 0.49, 0.37
N=27:	4.77, 4.15, 3.73, 3.41, 3.15, 2.93, 2.73, 2.55, 2.39, 2.25, 2.11, 1.97, 1.85, 1.73, 1.61, 1.49, 1.39, 1.29, 1.19, 1.09, 0.99, 0.89, 0.79, 0.69, 0.59, 0.49, 0.37
N=28:	4.83, 4.21, 3.79, 3.47, 3.21, 2.99, 2.79, 2.61, 2.45, 2.31, 2.17, 2.03, 1.91, 1.79, 1.67, 1.57, 1.47, 1.37, 1.27, 1.17, 1.07, 0.97, 0.87, 0.77, 0.67, 0.57, 0.47, 0.37
N=29:	4.89, 4.27, 3.87, 3.55, 3.29, 3.07, 2.87, 2.69, 2.53, 2.39, 2.25, 2.13, 2.01, 1.89, 1.77, 1.67, 1.57, 1.47, 1.37, 1.27, 1.17, 1.07, 0.97, 0.87, 0.77, 0.67, 0.57, 0.47, 0.37
N=30:	4.93, 4.31, 3.91, 3.59, 3.33, 3.11, 2.91, 2.73, 2.57, 2.43, 2.29, 2.17, 2.05, 1.93, 1.81, 1.71, 1.61, 1.51, 1.41, 1.31, 1.21, 1.11, 1.01, 0.93, 0.85, 0.77, 0.67, 0.57, 0.47, 0.37
N=31:	4.97, 4.35, 3.95, 3.63, 3.37, 3.15, 2.95, 2.77, 2.61, 2.47, 2.33, 2.21, 2.09, 1.97, 1.85, 1.75, 1.65, 1.55, 1.45, 1.35, 1.25, 1.15, 1.07, 0.99, 0.91, 0.83, 0.75, 0.67, 0.57, 0.47, 0.37
N=32:	4.99, 4.37, 3.97, 3.65, 3.39, 3.17, 2.97, 2.79, 2.63, 2.49, 2.35, 2.23, 2.11, 1.99, 1.87, 1.77, 1.67, 1.57, 1.47, 1.37, 1.27, 1.19, 1.11, 1.03, 0.95, 0.87, 0.79, 0.71, 0.63, 0.55, 0.45, 0.35
N=33:	5.03, 4.41, 4.01, 3.69, 3.43, 3.21, 3.01, 2.83, 2.67, 2.53, 2.39, 2.27, 2.15, 2.03, 1.93, 1.83, 1.73, 1.63, 1.53, 1.43, 1.35, 1.27, 1.19, 1.11, 1.03, 0.95, 0.87, 0.79, 0.71, 0.63, 0.55, 0.45, 0.35
N=34:	5.07, 4.45, 4.05, 3.75, 3.49, 3.27, 3.07, 2.89, 2.73, 2.59, 2.45, 2.33, 2.21, 2.09, 1.99, 1.89, 1.79, 1.69, 1.59, 1.49, 1.41, 1.33, 1.25, 1.17, 1.09, 1.01, 0.93, 0.85, 0.77, 0.69, 0.61, 0.53, 0.45, 0.35
N=35:	5.13, 4.51, 4.11, 3.81, 3.55, 3.33, 3.13, 2.95, 2.79, 2.65, 2.51, 2.39, 2.27, 2.15, 2.05, 1.95, 1.85, 1.75, 1.65, 1.57, 1.49, 1.41, 1.33, 1.25, 1.17,

1.09, 1.01, 0.93, 0.85, 0.77, 0.69, 0.61, 0.53, 0.45, 0.35
N=36: 5.19, 4.57, 4.17, 3.87, 3.61, 3.39, 3.21, 3.03, 2.87, 2.73, 2.59, 2.47, 2.35, 2.23, 2.13, 2.03, 1.93, 1.83, 1.73, 1.65, 1.57, 1.49, 1.41, 1.33, 1.25, 1.17, 1.09, 1.01, 0.93, 0.85, 0.77, 0.69, 0.61, 0.53, 0.45, 0.35
N=37: 5.23, 4.61, 4.21, 3.91, 3.65, 3.43, 3.25, 3.09, 2.93, 2.79, 2.65, 2.53, 2.41, 2.29, 2.19, 2.09, 1.99, 1.89, 1.79, 1.71, 1.63, 1.55, 1.47, 1.39, 1.31, 1.23, 1.15, 1.07, 0.99, 0.91, 0.83, 0.75, 0.67, 0.59, 0.51, 0.43, 0.35
N=38: 5.29, 4.67, 4.27, 3.97, 3.71, 3.49, 3.31, 3.15, 2.99, 2.85, 2.71, 2.59, 2.47, 2.35, 2.25, 2.15, 2.05, 1.95, 1.87, 1.79, 1.71, 1.63, 1.55, 1.47, 1.39, 1.31, 1.23, 1.15, 1.07, 0.99, 0.91, 0.83, 0.75, 0.67, 0.59, 0.51, 0.43, 0.35
N=39: 5.33, 4.71, 4.31, 4.01, 3.75, 3.53, 3.35, 3.19, 3.03, 2.89, 2.75, 2.63, 2.51, 2.39, 2.29, 2.19, 2.09, 1.99, 1.91, 1.83, 1.75, 1.67, 1.59, 1.51, 1.43, 1.35, 1.27, 1.19, 1.11, 1.03, 0.95, 0.87, 0.81, 0.73, 0.65, 0.57, 0.49, 0.41, 0.33
N=40: 5.33, 4.71, 4.31, 4.01, 3.75, 3.53, 3.35, 3.19, 3.03, 2.89, 2.75, 2.63, 2.51, 2.41, 2.31, 2.21, 2.11, 2.01, 1.93, 1.85, 1.77, 1.69, 1.61, 1.53, 1.45, 1.37, 1.29, 1.21, 1.13, 1.05, 0.97, 0.91, 0.85, 0.79, 0.73, 0.65, 0.57, 0.49, 0.41, 0.33
N=41: 5.33, 4.71, 4.31, 4.01, 3.77, 3.55, 3.37, 3.21, 3.05, 2.91, 2.77, 2.65, 2.53, 2.43, 2.33, 2.23, 2.13, 2.03, 1.95, 1.87, 1.79, 1.71, 1.63, 1.55, 1.47, 1.39, 1.31, 1.23, 1.15, 1.07, 1.01, 0.95, 0.89, 0.83, 0.77, 0.71, 0.65, 0.57, 0.49, 0.41, 0.33
N=42: 5.37, 4.75, 4.35, 4.05, 3.81, 3.59, 3.41, 3.25, 3.09, 2.95, 2.81, 2.69, 2.57, 2.47, 2.37, 2.27, 2.17, 2.07, 1.99, 1.91, 1.83, 1.75, 1.67, 1.59, 1.51, 1.43, 1.35, 1.27, 1.19, 1.13, 1.07, 1.01, 0.95, 0.89, 0.83, 0.77, 0.71, 0.65, 0.57, 0.49, 0.41, 0.33
N=43: 5.39, 4.77, 4.37, 4.07, 3.83, 3.61, 3.43, 3.27, 3.11, 2.97, 2.83, 2.71, 2.59, 2.49, 2.39, 2.29, 2.19, 2.09, 2.01, 1.93, 1.85, 1.77, 1.69, 1.61, 1.53, 1.45, 1.37, 1.29, 1.23, 1.17, 1.11, 1.05, 0.99, 0.93, 0.87, 0.81, 0.75, 0.69,

0.63, 0.57, 0.49, 0.41, 0.33
N=44: 5.43, 4.81, 4.41, 4.11, 3.87, 3.65, 3.47, 3.31, 3.15, 3.01, 2.87, 2.75, 2.63, 2.53, 2.43, 2.33, 2.23, 2.13, 2.05, 1.97, 1.89, 1.81, 1.73, 1.65, 1.57, 1.49, 1.41, 1.33, 1.27, 1.21, 1.15, 1.09, 1.03, 0.97, 0.91, 0.85, 0.79, 0.73, 0.67, 0.61, 0.55, 0.49, 0.41, 0.33
N=45: 5.47, 4.85, 4.45, 4.15, 3.91, 3.69, 3.51, 3.35, 3.19, 3.05, 2.91, 2.79, 2.67, 2.57, 2.47, 2.37, 2.27, 2.17, 2.09, 2.01, 1.93, 1.85, 1.77, 1.69, 1.61, 1.53, 1.45, 1.39, 1.33, 1.27, 1.21, 1.15, 1.09, 1.03, 0.97, 0.91, 0.85, 0.79, 0.73, 0.67, 0.61, 0.55, 0.49, 0.41, 0.33
N=46: 5.51, 4.89, 4.49, 4.19, 3.95, 3.73, 3.55, 3.39, 3.23, 3.09, 2.97, 2.85, 2.73, 2.63, 2.53, 2.43, 2.33, 2.23, 2.15, 2.07, 1.99, 1.91, 1.83, 1.75, 1.67, 1.59, 1.51, 1.45, 1.39, 1.33, 1.27, 1.21, 1.15, 1.09, 1.03, 0.97, 0.91, 0.85, 0.79, 0.73, 0.67, 0.61, 0.55, 0.49, 0.41, 0.33
N=47: 5.53, 4.91, 4.51, 4.21, 3.97, 3.75, 3.57, 3.41, 3.25, 3.11, 2.99, 2.87, 2.75, 2.65, 2.55, 2.45, 2.35, 2.25, 2.17, 2.09, 2.01, 1.93, 1.85, 1.77, 1.69, 1.61, 1.55, 1.49, 1.43, 1.37, 1.31, 1.25, 1.19, 1.13, 1.07, 1.01, 0.95, 0.89, 0.83, 0.77, 0.71, 0.65, 0.59, 0.53, 0.47, 0.41, 0.33
N=48: 5.57, 4.95, 4.55, 4.25, 4.01, 3.79, 3.61, 3.45, 3.29, 3.15, 3.03, 2.91, 2.79, 2.69, 2.59, 2.49, 2.39, 2.31, 2.23, 2.15, 2.07, 1.99, 1.91, 1.83, 1.75, 1.67, 1.61, 1.55, 1.49, 1.43, 1.37, 1.31, 1.25, 1.19, 1.13, 1.07, 1.01, 0.95, 0.89, 0.83, 0.77, 0.71, 0.65, 0.59, 0.53, 0.47, 0.41, 0.33
N=49: 5.59, 4.99, 4.59, 4.29, 4.05, 3.83, 3.65, 3.49, 3.33, 3.19, 3.07, 2.95, 2.83, 2.73, 2.63, 2.53, 2.43, 2.35, 2.27, 2.19, 2.11, 2.03, 1.95, 1.87, 1.79, 1.73, 1.67, 1.61, 1.55, 1.49, 1.43, 1.37, 1.31, 1.25, 1.19, 1.13, 1.07, 1.01, 0.95, 0.89, 0.83, 0.77, 0.71, 0.65, 0.59, 0.53, 0.47, 0.41, 0.33
N=50: 5.63, 5.03, 4.63, 4.33, 4.09, 3.87, 3.69, 3.53, 3.37, 3.23, 3.11, 2.99, 2.87, 2.77, 2.67, 2.57, 2.47, 2.39, 2.31, 2.23, 2.15, 2.07, 1.99, 1.91, 1.83, 1.77, 1.71, 1.65, 1.59, 1.53, 1.47, 1.41, 1.35, 1.29, 1.23, 1.17, 1.11, 1.05, 0.99, 0.93, 0.87, 0.81, 0.75, 0.69, 0.63, 0.57, 0.51, 0.45, 0.39, 0.31

References

(S1) Shockley, W.; Queisser, H. J. Detailed Balance Limit of Efficiency of p-n Junction Solar Cells. *Journal of Applied Physics* **1961**, *32*, 510–519.

(S2) Green, M. A. Efficiency limits for single-junction and tandem solar cells. *Progress in Photovoltaics: Research and Applications* **2006**, *14*, 383–395.

(S3) Rau, U.; Paetzold, U. W.; Kirchartz, T. Thermodynamics of light management in photovoltaic devices. *Physical Review B* **2014**, *90*, 035211.

(S4) Rau, U.; Kirchartz, T. Efficiency potential of photovoltaic materials and devices unveiled by detailed-balance analysis. *Physical Review B* **2017**, *95*, 245201.

(S5) Rau, U. Reciprocity relation between photovoltaic quantum efficiency and electroluminescent emission of solar cells. *Physical Review B* **2007**, *76*, 085303.

(S6) Miller, O. D.; Yablonovitch, E. Strong internal and external luminescence as solar cells approach the Shockley–Queisser limit. *IEEE Journal of Photovoltaics* **2012**, *2*, 303–311.

(S7) Kirchartz, T.; Rau, U. What makes a good solar cell? *Advanced Energy Materials* **2018**, *8*, 1703385.

(S8) Reich, N.; Yu, Y.; Furchi, M.; others Efficiency limit of transition metal dichalcogenide solar cells. *Communications Physics* **2023**, *6*, 1–11.

(S9) Jariwala, D.; Davoyan, A. R.; Wong, J.; Atwater, H. A. Van der Waals Materials for Atomically-Thin Photovoltaics: Promise and Outlook. *ACS Photonics* **2017**, *11*, 53–61.

(S10) Zhou, Z.; Lv, J.; Tan, C.; Yang, L.; Wang, Z. Emerging Frontiers of 2D Transition Metal Dichalcogenides in Photovoltaics Solar Cell. *Advanced Functional Materials* **2024**, *34*, 2316175.

(S11) Yu, Z.; Raman, A.; Fan, S. Fundamental limit of nanophotonic light trapping in solar cells. *Proceedings of the National Academy of Sciences* **2010**, *107*, 17491–17496.

(S12) Miller, D. A. B. Why optics needs thickness. *Science* **2023**, *380*, 742–746.

(S13) Park, Y.; Zhao, B.; Fan, S. Reaching the Ultimate Efficiency of Solar Energy Harvesting with a Nonreciprocal Multijunction Solar Cell. *Nano Letters* **2022**, *22*, 448–452.

(S14) Park, Y.; Fan, S. Does Non-Reciprocity Break the Shockley–Queisser Limit in Single-Junction Solar Cells? *Applied Physics Letters* **2022**, *121*, 111102.